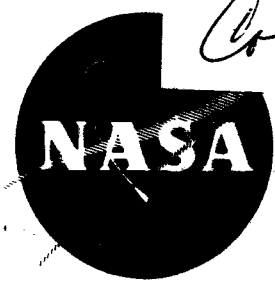

EXPERIMENTAL NEUTRON FLUX DISTRIBUTIONS IN A WATER SYSTEM WITH AN INTERNAL CAVITY

by

FLORO MIRALDI, DAVID McBRIDE, AND GEORGE W. NELSON

prepared for

NATIONAL AERONAUTICS AND SPACE ADMINISTRATION

CONTRACT NAS 3-3213

CASE INSTITUTE OF TECHNOLOGY

NOTICE

This report was prepared as an account of Goverment sponsored work. Neither the United States, nor the National Aeronautics and Space Administration (NASA), nor any person acting on behalf of NASA:

A.) Makes any warranty or representation, expressed or implied, with respect to the accuracy, completeness, or usefulness of the information contained in this report, or that the use of any information, apparatus, method, or process disclosed in this report may not infringe privately owned rights, or

B.) Assumes any liabilities with respect to the use of, or for damages resulting from the use of any information, apparatus, method or process disclosed in this report.

As used above, "person acting on behalf of NASA" includes any employee or contractor of NASA, or employee of such contractor, to the extent that such employee or contractor of NASA, or employee of such contractor prepares, disseminates, or provides access to, any information pursuant to his employment or contract with NASA, or his employment with such contractor.

Requests for copies of this report should be referred to

National Aeronautics and Space Administration
Office of Scientific and Technical Information
Attention: AFSS-A
Washington, D.C. 20546

NASA CR-54110

FINAL REPORT

EXPERIMENTAL NEUTRON FLUX DISTRIBUTIONS IN A WATER SYSTEM WITH AN INTERNAL CAVITY

by

Floro Miraldi, David A. McBride, and George W. Nelson

prepared for

NATIONAL AERONAUTICS AND SPACE ADMINISTRATION

June 30, 1964

CONTRACT NAS-3213

Technical Management
NASA Lewis Research Center
Cleveland, Ohio
Nuclear Reactor Division
Eldon W. Sams

Case Institute of Technology
Cleveland, Ohio

EXPERIMENTAL NEUTRON FLUX DISTRIBUTIONS IN A WATER SYSTEM WITH AN INTERNAL CAVITY

by

Floro Miraldi, David A. McBride, and George W. Nelson

ABSTRACT

Neutron flux distributions were measured in a system consisting of a large spherical cavity in water. Three cavity geometries were studied including concentric sphere systems. Cavity fillings were air at one atmosphere and BF_3 at various pressures between one and three atmospheres. Measurements were made by foil activation. Foil activation distributions are presented, and relative thermal flux distributions are compared to Fermi-Age and Two-Group diffusion theory. Results show that the flux distributions in the cavity regions are quite flat. Comparisons of theory and experiment indicates that the simple calculations performed are insufficient to describe these systems.

EXPERIMENTAL NEUTRON FLUX DISTRIBUTIONS IN A WATER SYSTEM WITH AN INTERNAL CAVITY

by F. Miraldi, D. A. McBride and G. W. Nelson

Case Institute of Technology

SUMMARY

Experimental neutron flux distributions were measured in a water filled tank containing a 27-inch diameter spherical cavity region. Neutrons were provided by a plutonium-beryllium neutron source located at the center of the cavity, and bare and cadmium-covered indium foils were used to determine the neutron flux distributions in both the cavity and moderator regions. Three separate cavity systems were examined including the simple cavity, a concentric sphere system with a 9-inch diameter interior sphere, and a concentric sphere system with a 12-inch diameter interior sphere.

Foil activation distributions and thermal neutron flux distributions are presented for the several cavity cases examined. These included cavity fillings of boron trifluoride gas to simulate a uranium hexafluoride gas-filled cavity. In the concentric sphere cases only the interior sphere was filled with boron trifluoride to simulate fuel contraction, and for these, various gas pressures were used to investigate the effects of increased absorption in the cavity. An air-filled cavity and a no cavity case were studied for comparative purposes. The general shapes of the distributions are as expected except toward the center of the cavity where a slight flux peaking occurs in some situations.

Simple two-group diffusion and Fermi-Age calculations were made for the expected thermal neutron distributions. Agreement between the experiment and calculations was not good as was anticipated for such approximate theories. author

INTRODUCTION

Reactors consisting of a low density interior region surrounded by an external reflector-moderating region have attracted considerable interest in recent years. This reactor type has been referred to as a "cavity reactor." In one basic concept, the gaseous core reactor, fuel is contained in the interior region as a fissionable gas. This particular concept is of interest in the space program because of its potential as a high performance propulsion engine. Interest in the use of these devices as propulsion units arises from the fact that most of the fission energy appears as kinetic energy of the fission fragments. These fragments have extremely short mean free paths in matter which means that most of the fission energy is dissipated essentially at the site of fission. By mixing a propellant with the fissioning gas, high gas temperatures may be achieved yielding large specific impulses. A number of such devices have been propsed and described in the literature. (1-8).

The nucleonics of the cavity reactor was first described by Bell (9) who investigated a class of systems employing UF_6. Safanov (10) has made a rather extensive survey of spherical reactors with the cavity region completely and uniformly filled with a gaseous fuel. His approach utilized Fermi-Age theory and is comparable to that of Bell. Multigroup diffusion calculations have been performed by Ragsdale and Hyland (11,12) and by Plunkett and Holl (13). Mills (14) has performed S_n calculations and has shown excellent agreement between experimental critical masses and calculational results.

There has been, on the other hand, very little experimental data accumulated on these systems. A critical assembly consisting of a U-235-foil-lined cylindrical tank surrounded by D_2O was constructed at Los Alamos. Radial and axial flux traverses in the cavity were reported by Paxton and Orndoff (15). Fox et al (16) measured the neutron flux distributions in a graphite assembly with an internal

cavity of cubic shape. The system employed a Po-Be neutron source and studied the cases of an air-filled and one-atmosphere, BF_3-filled cavity. Their results were compared to an 18-energy-group, one-dimensional, spherical-geometry calculation and found to agree well.

The work reported herein was undertaken to provide additional experimental data regarding neutron diffusion in cavity media. In many respects this work is an extension of that of Fox et al. The primary objective of this study was the measurement of neutron flux distributions in a cavity filled with a neutron absorbing gas under different pressures and geometry. The external moderating media was chosen to be water which provided a significantly different situation than the one studied by Fox et al. The cavity geometry was spherical to facilitate comparison with theory and the neutrons were provided by a Pu-Be source placed at the center of the system. As in the experiments of Fox et al, boron trifluoride gas was used as cavity filling because it closely approximates the thermal neutron absorption properties of uranium hexafluoride gas. In contrast, however, the cavity filling was not always uniform and the gas pressure was varied. Non-uniformity was accomplished by filling a smaller sphere with BF_3 and placing the sphere inside and concentric with the cavity. This corresponds to a rocket concept in which the fuel region is compressed by hydrodynamic or magnetic means in the cavity interior.

Though this study was primarily experimental, a limited analytical investigation was performed to compare the results to theory. The analysis performed was a simple two-group diffusion calculation and a Fermi-Age treatment as developed by Safanov (10).

DESCRIPTION OF EQUIPMENT AND EXPERIMENTAL PROCEDURE

The Experimental Assembly

The overall experimental setup is shown in Figure 1 for a concentric sphere system with a 12 inch inner sphere. The external

moderating media was deionized water at room temperature contained in a stainless steel cylindrical tank approximately four feet in diameter by four feet high.

The spherical cavity interior region was formed from two flanged aluminum hemispheres welded together. The hemispheres were 2S aluminum about 1/16 inch thick and 27 inches in diameter. The sphere was centered in the water tank and held in position by 1/4 inch vertical aluminum rods connected to the sphere flang and anchored to the bottom of the tank. A thru-tube about 1 1/8 inch in internal diameter and approximately 1/16 inch thick was provided to allow the insertion of the neutron source and foils into the system. The thru-tube pierced the entire system along the sphere diameter and extended several inches beyond the water tank boundary. The thru-tube was welded to the sphere and attached to the tank by couplings. To eliminate large flux perturbations, the coupling was accomplished by butt joining the tubes and taping them. Structural strength was obtained by providing splints over the tape which were in turn taped into position. The sphere shell was provided with three ports about 2 inches in diameter to allow access for foil positioning as an alternate to the thru-tube. Photographs of the sphere system are presented in Figure 2.

Three separate sphere systems were constructed identical to the one described except that two of the systems contained a concentric inner sphere. The inner spheres had diameters of 9 inches and 12 inches and were about 1/16 inch thick also. The 12 inch inner sphere system is shown by the cut-away of Figure 1. These inner spheres were constructed by welding two hemispheres together and were held in place by welding to the thru-tube.

The spheres were evacuated or filled via a gas channel through the thru-tube connector of the outer sphere. In the concentric sphere systems, aluminum tubing was used to carry the gas along the outside of the thru-tube into the inner sphere. Teflon tubing was used to connect the gas supply to the gas inlet to the sphere and mercury manometers were used to regulate pressure.

Because of the highly corrosive nature of BF_3 in the presence of moisture, the spheres were evacuated and vacuum held for several hours to insure removal of all water vapor before admitting the BF_3 into the system. Although many problems were experienced in initially pressurizing the spheres with BF_3, no problem was experienced in maintaining a constant pressure during the runs.

Neutron Source, Detecting Foils and Holders

The plutonium-beryllium source used was a standard model Mound Laboratory source in the shape of a cylinder. Details of the source construction are given in Figure 3. The source material was doubly canned in tantalum and stainless steel and occupied about four-fifths of the internal volume. The external dimensions were about one inch in diameter and 1.6 inches in length. The neutron emission was about 1.7×10^6 neutrons per second. The source was admitted into the cavity via the thru-tube and centered by measuring along the interior of the thru-tube. Orientation of the source was always the same to eliminate the possibility of error due to non-uniformity of the neutron emission. Checks of the data indicated, though, that such non-uniformity was beyond the limits of detection by the methods employed in this study.

The indium foils used were circular disks approximately one inch in diameter and 5 mils thick and had a weight of about 92 milligrams per square centimeter. The indium was chemically pure to better than 99.9%. The foils were carefully weighed to 0.1 milligram and a set of closely identical foils were used. The cadmium covers were made from chemically pure cadmium and had a nominal thickness of 20 mils.

Three different holder systems were used for the foils and photographs of them are presented in Figure 4. One set of holders for use in the thru-tube consisted of a small aluminum ring with an internal flange against which the foils were held by a second small ring which fit snugly inside the first. (Fig. 4a). The foil holders were positioned along the thru-tube by the use of accurately

machined spacers placed between the holders. The same holders were fixed to a support and the rig attached to a port cap in order to obtain readings in positions other than in the thru-tube (Fig. 4b). The third type of foil holder was a standard commerical holder consisting of a lucite ring with a thin plastic backing and a screw-on plastic cap (Fig. 4c). The foil was placed in the ring between the backing and cap and the assembly was supported on a lucite rod. Foils were placed in these holders for measurements in the water. The relative positions of the foil holders in the experiment is shown in Fig. 1. Foils were also positioned on the outside surface of the spheres and on the inside surface of the outer sphere. Access to the inside surface of the outer sphere was through the 2 inch ports. These foils were held in position with ordinary cellophane tape.

From a practical point of view it was necessary to expose many foils at the same time; though the possibility of flux perturbation effects of one foil on another was recognized. Calculations based on the developments of Vigon and Wirtz and of Meister (17) indicated that a minimum separation of foils of about 2 inches was necessary to reduce this interference effect below one percent. In all cases in this study a minimum separation of four inches in the cavity region and three inches in the water region was maintained so that these effects would be negligible compared to other experimental errors.

The foils were always exposed for periods greater than six hours to activate them to saturated values of the 54.3 minute activity. They were counted twice, once in a Geiger-Mueller, end-window counter and once in a gas-flow, proportional counter with 4π geometry. This was done to facilitate the tracking of error or malfunction of equipment. All data reported herein, however, is that obtained with the 4π counter since the scatter of data was slightly less for this system.

BF_3 Proportional Counters

Some measurements were made using BF_3 proportional counters

because they offered fast checks on the flux distributions. In general these runs were done for internal checks and the data is not sufficiently complete to be reported. They are mentioned because reference is made to two runs in the section to follow. Two Wood Co. probes were used for these runs; one 7/8 inch diameter with active length of one inch and the other 1 1/8 inch diameter with an active length of two inches. The gas filling pressures of $B^{10}F_3$ of the probes was 60 cm of mercury and 20 cm of mercury respectively. The probes were positioned either in the thru-tube or in a similar aluminum tube along the position shown in Figure 1 for the water foil holder.

EXPERIMENTAL RESULTS

This section presents the experimental results obtained for the various cases studied. These include

(1) Air-filled cavity
(2) Single cavity with one atmosphere BF_3 filling
(3) Concentric sphere system with 12 inch inner sphere and BF_3 fillings of 1, 2, and 2.5 atmospheres in the inner sphere
(4) Concentric sphere system with 9 inch inner sphere and BF_3 fillings of 1, 2, and 3 atmospheres in the inner sphere
(5) No cavity

The results are presented as graphs in two parts: first as relative foil activation distributions and then as relative thermal flux distributions. This section begins with general comments about the results and follows with a discussion of particular cases. The section is concluded by a discussion of the data reduction procedure and the experimental precision.

General Comments

In the following, results for the interior region were based on data obtained in the thru-tube except for regions close to the

moderator boundary. Data obtained via the ports agreed very well with the thru-tube data and indicate that in the interior region the thru-tube effects were less than the limits of the experimental precision.

The data obtained in the thru-tube in the water region agreed generally in shape with that obtained from the foils irradiated in the lucite holders* but differed slightly in magnitude. Deviations in the shape occurred near the water tank boundary and near the cavity boundary. The former deviations are attributed to neutron streaming from the tube. Near the cavity boundary the effect is attributed to the fact that neutron thermalization is not as rapid with distance in the vicinity of the tube as it is in the water. Because the in-water data is the desired data, all graphs but two were prepared from the in-water results. The exceptions occurred because a time limitation prevented the accumulation of the in-water data for these cases. Cavity boundary data obtained from foils activated at the inner and outer surfaces of the cavity agreed well with the extrapolations of the in-water data to the cavity boundary. The tube results in the water region are presented in several cases to illustrate the differences.

Generally, several exposures were made at each position for each case and the results plotted are the average values. Various causes required the elimination of some data and unnecessary duplication of other data so that the number of values averaged varied from point to point.

Foil Activation Distributions

The foil activation data is presented in Figures 5 through 18. Figures 5 through 13 show the results for individual cases and Figures 14 through 18 present comparative curves for the

---

* This data will be referred to as in-water data in the following.

different cases. Continuous curves drawn through the data points are passed through the tube data in the interior region and through the in-water data in the water region. The broken line curve in the water region represents the thru-tube data except in Figures 12 and 13 (cases of the 9 inch inner sphere with 2 and 3 atmospheres of BF_3). For these latter cases only thru-tube data was obtained and the continuous curve was passed through these results; the broken line curve represents an estimate of what the in-water data might be.

Figure 5 presents the cadmium covered foil data. It was assumed that all cavities, whether air or BF_3 filled, were voids to the higher energy neutrons. Hence, the cadmium covered data from all runs was averaged to yield a "best" curve. A sharp peaking is noted in this foil data near the source. It has been suggested (16) that this peaking arises from the 54-minute indium activation due to uncollided and once collided source neutrons.

In Figure 6 the foil activations for an air filled cavity is presented. Although three different sphere systems were examined, no apparent difference was observed. In the experiments of Fox et al (16), the presence of an aluminum liner at a cavity boundary caused a noticable depression in the magnitude of the thermal flux. This effect was apparently masked in this study for two reasons. These studies employed a water moderator which has an absorption cross section larger than aluminum in contrast to the experiment of Fox which employed graphite where the absorption cross section is about two orders of magnitude lower than aluminum. Hence, the aluminum liner in their case constituted an appreciable relative absorption. Secondly, the addition of an inner sphere to the cavity constituted an increase in aluminum to the system which was only a fraction of the amount normally present.

A peaking effect at the sphere center is also observed in Figures 6 and 7; though in these cases it is more gradual and not as pronounced. It is tempting to attributed this effect to the same cause suggested for the cadmium covered foils since the magnitude of the peak is the same in all three cases.

A large depression in the cavity and a large peak in the water are the most striking features of Figure 7 which shows the case of the entire cavity filled to one atmosphere of BF_3. This peak and depression are expected because of the large amount of BF_3 contained in the cavity in this case. The difference between thru-tube data and in-water data is also most pronounced for this situation.

In Figures 8, 9, and 10 the water peaking essentially disappears because of the much smaller absorption in the 12 inch inner sphere compared to the single sphere system. The same occurred for the 9 inch inner sphere system as demonstrated by Figures 11, 12, and 13. A particular feature is of note in the cases of inner spheres; namely, the gradual decrease in values through the void region in going from moderator to inner sphere.

For all the activity curves the typical exponential drop-off of the values in the water region is noted. The value at one inch distance is significantly lower in all cases involving the bare foil activations. The cause of this depression is apparently the depression of the thermal flux due to the absorption of the source.

The comparative graphs, Figures 14 through 18, were prepared from the continuous curves of the previously mentioned cases except for the 9 inch inner sphere systems with 2 and 3 atmospheres of BF_3. The estimated in-water data was used for graphs involving these latter cases.

The similarity of the curves and essential equality of values in the water region beyond a few inches from the cavity boundary is apparent from the comparisons. No unusual characteristics are exhibited in these graphs over those previously mentioned, and the trends appear to be well mannered and as expected.

Flux Distributions

The relative neutron flux distributions were obtained from the activation data and are presented in Figures 19 through 26. The relative fast (epicadmium) flux is given by the cadmium-covered foil data. The relative thermal flux was obtained as the difference of the bare foil data and cadmium covered data corrected for flux depression and resonance absorption by the cadmium. Values used in the thermal flux plots were read from the smooth curves drawn through the data points and not the actual data points themselves. The cadmium correction factor used was 1.07 and the flux depression correction factors used were 1.00 in the cavity region and 1.18 in the water region. These correction factors are discussed in Appendix I.

Figure 19 compares the thermal flux of an air filled cavity to the case of no-cavity. The droop of the no-cavity case in the vicinity of the source is explained as source absorption of thermal neutrons. The very large flux depression caused by the presence of the cavity is well illustrated in this figure. Though the flux distribution is quite flat in the cavity, attention is directed to the gradual peaking toward the center. Figure 20 presents BF_3 neutron counter data for the air filled cavity case. Since boron is a 1/v absorber which exhibits little resonance structure, the counter count-rate is essentially proportional to the slow flux. It will be noted that the gradual rise in value toward the center is apparent again.

Figure 21 presents a comparison of the thermal flux of the air filled cavity with the cavity completely filled with BF_3 and compares both of these with the fast flux. The peaking of the flux for the BF_3 filling is more pronounced than in the foil data case because of an apparent inflection in the curve at about 5 inches. BF_3 counter data for this same case is shown in Figure 22 where it will be seen that such a peaking does not occur. This places some question on the existance and meaning of the effect shown in Figure 20.

In the remaining flux graphs, Figures 23 through 26, the thermal flux behavior is similar to the corresponding bare foil activation except for the increase in peaking effect in the water which arises because of the depression correction of 1.18.

Reduction of Experimental Foil Data

Many simplifications were possible in this work since only relative data were needed. Additional reduction of the number of corrections needed were possible in many cases by employing certain experimental techniques such as using a constant count period and exposing the foils to saturation values.

The basic corrections employed were:

(1) Correction for the decay of the foil activity during the time between the end of foil exposure and start of counting.

(2) Correction for the decay of the foil activity during foil counting.

(3) Correction for counting equipment background.

(4) Correction for the long (4.5 hour) half life activation of foils located near the source.

(5) Correction for the difference in foil weights.

(6) Correction for capture of resonance neutrons by the cadmium covers.

(7) Correction for the difference in thermal flux depression between media.

Counter resolving time corrections were not necessary because of the low count rates involved. Other corrections often employed, such as finite size source and detector corrections, were not considered appropriate for the presentation here and therefore were not applied.

The foil data were all normalized to the saturated value of the 54-minute activity. Details on the method of applying the above mentioned corrections are given in Appendix I.

Experimental Errors

It is extremely difficult to rigorously perform an error analysis of the data of this report. However, it should be noted that such an analysis is not needed for the results to have meaning because the nature of the data does not require extreme accuracy. Therefore the short discussion here is presented very loosely.

In general, for the bare foil data, the deviations of the data points in the cavity region from the smooth curve ranged from a low of about $\pm$ 0.5% to a maximum of approximately $\pm$ 5% . On the average deviations were on the order of $\pm$ 1% These numbers do not include the large deviation at the one inch spacing. A typical point in this region has a standard deviation due to counting statistics alone of approximately $\pm$ 1%. Thus in the cavity region the variations in the bare foil results appear to be due primarily to the counting statistics.

In the water region, the average deviation of the data from the curve ranges from about $\pm$1% at regions close to the cavity boundary to about $\pm$ 3.5% at regions midway through the medium. Again the effects are primarily due to counting statistics

since typical values yield a standard deviation of about $\pm$ 1 % in the vicinity of the cavity and about 2.5 in the midway region. Close to the tank boundary where the count rates were quite low, the deviations become quite high and the shape of the distribution much more uncertain.

The results for the cadmium covered foils indicate much larger deviations as is expected since the count rates are an order of magnitude lower than for the bare foils. The average deviation of data points from the curve is approximately $\pm$ 5.5 %. Typical count rates in the cavity region yield a standard deviation due to counting statistics of $\pm$ 4 % and in the water region the standard deviation ranges from about $\pm$ 4 % for regions close to the cavity to $\pm$ 30 % for regions near the tank boundary.

Therefore it appears that throughout the experiment, the variations exhibited by the foil data can be attributed primarily to counting statistics. Although in some instances the variations may be large, the significance of the results are not seriously affected.

COMPARISON OF THEORY AND EXPERIMENT

Calculations were peformed based on Fermi-Age theory and two-group diffusion theory. The Fermi-Age calculationswere based on the developments of Safanov (10), and the two-group results are developed in Appendix II. Because the moderator region had a minimum thickness of 10.5 inches, which is large compared to the diffusive characteristics of neutrons in water, the approximation of an infinite external region was made.

The interior fluxes in both theories are obtained from the results of Safanov. He used the P_1 approximation for the directional flux ψ at the surface of the cavity and integrated (ψ times the noncapture probability associated with neutron

flight into the interior) over the cavity surface.

For the concentric sphere systems with BF_3 fillings, a current conservation condition was used in which the net neutron flow from the moderator into the cavity was equated to the net flow into the inner cavity. In diffusion theory this procedure results in a flat flux between spheres.

The results of the computations are presented along with the experimentally determined values in Figures 27 through 34. In all cases it is observed that the experimental values lie between the Fermi-Age and two-group results in the water region. The position of the flux peak in the water is closely predicted by the two-group approximation but rather poorly predicted by the Fermi-Age treatment. The flux depression in the BF_3 cavities is underestimated by the analytical results. This is perhaps an untrue comparison since the neutron absorption by the neutron source was not take into account. The notable exception to this latter statement is illustrated in Figure 28, no inner sphere with one atmosphere of BF_3 filling, which has received prior mention. If, in this case, the BF_3 counter data is used, the experimental and Fermi-Age results compare quite well.

In summary it appears that the simple analyses performed do not predict the experimental results well. It must be admitted, however, that the comparisons are not completely fair since the calculations did not consider the high absorption of the neutron source. Modification of the calculations are presently being considered by the authors.

APPENDIX A

CORRECTIONS REQUIRED FOR DATA REDUCTION

The corrections applied to the raw data were stated previously. These procedures are fairly standard to foil work and this discussion is presented primarily for the convenience of the reader and to provide additional details to clarify the particular approach employed in this study.

Indium Activities Considered

The relative count rates which were plotted represent the 54.3 minute actvity of indium. This is the usual activity chosen because of the large cross section for its formation and the convenient half-life. Other activities are produced in an experiment of this type, however, and must be considered.

Natural indium consists of two isotopes, In-113 and In-115, both of which yield radioactive indium upon neutron exposure. In-113, though, is present only to the extent of 4.23% (18), and since its activation cross sections are relatively small, it is neglected here.

Neutron exposure of In-115 yields three different activities with half-lives of 13 seconds, 54.3 minutes, and 4.50 hours (18). In this study all foils were allowed to cool for ten minutes before counting so that the 13 second activity was not of concern. The long half-life isomer is produced by inelastic collisions of neutrons with energies greater than about one Mev. Therefore, in regions close to the neutron source where the high energy flux was large, this activity was significant and corrections had to be applied.

Relative Activity Corrections

The plotted quantities labeled "relative activities" are really activity values averaged over a short time interval and normalized to the saturated value of the 54.3 minute activity per unit weight. In the following the expression actually plotted is developed to clarify the corrections used.

If $A(t, \theta)$ is the activity of a foil at time t following an irradiation for a time period θ, then the count rate observed, C, is given as $C = \alpha A + B$, where B is the background count rate of the instrument and α is a proportionality factor which depends upon counter efficiency, stability, and geometry. In this study all instrument factors and geometry were maintained constant so that α was a constant for all foils. The quantity α was checked frequently during runs by examining the count rate from standard foils. Instrument stability and geometry reproducibility were sufficiently good so that corrections on α were found unnecessary.

The data accumulated, K, were the total counts observed over an interval of time

$$K = \int_{t_1}^{t_2} C \, dt$$

where t_1 was the time from the end of exposure to the start of the count and t_2 was the time from the end of exposure to the end of the count.

The activity A is composed of two parts

$$A = A_S(\theta)\, e^{-\lambda_S t} + A_L(\theta)\, e^{-\lambda_L t}$$

where the subscripts S and L refer to the short and long half-lives respectively, $A(\theta)$ is the activity after a neutron exposure for the time θ, and λ is the radioactive decay constant. The activities $A(\theta)$ are, in turn, given by

$$A_S(\theta) = \alpha_S W \left(1 - e^{-\lambda_S \theta}\right)$$

$$A_L(\theta) = \alpha_L W \left(1 - e^{-\lambda_L \theta}\right)$$

where W is the foil weight and α_S and α_L are proportionality factors dependent upon activation cross sections and average flux values in the foil. In all the runs, θ was much larger than the short half-life and hence $A_S(\theta)$ was taken as $\alpha_S W$. Thus it is seen that

$$C = \alpha\alpha_S W e^{-\lambda_S t} + \alpha\alpha_L W \left(1 - e^{-\lambda_L \theta}\right) e^{-\lambda_L t} + B$$

and

$$K = \frac{\alpha\alpha_S W}{\lambda_S}\left(e^{-\lambda_S t_1} - e^{-\lambda_S t_2}\right) + \frac{\alpha\alpha_L W}{\lambda_L}\left(e^{-\lambda_L t_1} - e^{-\lambda_L t_2}\right)\left(1 - e^{-\lambda_L \theta}\right) + B\,(t_2 - t_1)$$

It should be noted here that the quantity of interest is the (slow) neutron flux which is contained in α_S.

It is convenient to form the quantity D as

$$D = \frac{1}{W}\left[\frac{K}{(t_2 - t_1)} - B\right] e^{\lambda_S t_1}$$

$$= K_S\left[1 + \frac{K_L}{K_S}\left(1 - e^{-\lambda_L \theta}\right) e^{(\lambda_S - \lambda_L) t_1}\right]$$

where

$$K_S = \frac{\alpha\alpha_S}{\lambda_S \delta}\left(1 - e^{-\lambda_S \delta}\right)$$

$$K_L = \frac{\alpha\alpha_L}{\lambda_L \delta}\left(1 - e^{-\lambda_L \delta}\right)$$

$$\delta = (t_2 - t_1)$$

Throughout most of the system the second term in the bracket above is negligible and hence $D \approx K_S$. The quantity K_S is

directly proportional to α_S for constant counting periods δ. For most counts, δ was taken as 10 minutes; however, where longer periods were required, the results were normalized to the 10 minute period by adjusting the values of K_S and K_L. The graphs of the activies are plots of K_S which, for most cases, is equal to D and computed directly from the raw count data, K. The correction for K_L not negligible is given below.

The quantity K_S is proportional to the average flux through α_S. For the bare foils, this average is over all foil positions and all neutron energies. In the case of the cadmium covered foils, the energy average extends down only to the cadmium cutoff energy.

In those situations where the long half-life activity was significant, K_S was obtained as

$$K_S = D \left[1 + \frac{K_L}{K_S} \; 1 - e^{-\lambda_L \theta} \; e^{(\lambda_S - \lambda_L) t_1} \right]^{-1}$$

$$= D \, \eta$$

and η was obtained by experimentally measuring the ratio (K_L/K_S). This latter ratio was obtained by following the decay activity of a foil for longer periods, decomposing the decay curve into its two components, and extrapolating the component curves back to $t_1 = 0$. The ratio of the zero intercept of the long half-life component to the intercept of the short half-life componenent is the ratio (K_L/K_S). Figure (35) is a plot of (K_L/K_S) for cadmium covered foils.

For the case of the cadmium covered foils, the long half-life correction is large close to the source but drops off very rapidly. For these foils, the corrections was applied out to a distance of five inches.

The total activations of the bare foils are an order of magnitude higher than for the cadmium covered foils. The long half-life activity, however, would remain about the same in both cases and hence is a correction of only a few percent at most for the bare foils. The tedious procedure for obtaining

the long half-life correction used with the cadmium covered foils was not followed in the bare foil runs. Instead, this correction was estimated by assuming that the long half-life activity would be the same whether a foil were bare or covered. Therefore the value of K_L obtained from the cadmium covered data was used for the bare foils as well. The error incurred by this procedure is not expected to exceed a fraction of one percent. It was not necessary to apply this correction beyond three inches from the source for the bare cases.

Flux Depression Corrections

The flux perturbation factor is the ratio of the neutron activation of a foil of finite size (for which the flux is perturbed) to that of the same foil if there were no flux perturbation. In practice it is not possible to achieve the latter condition and it has become common procedure to use the so-called infinitely thin foil; i.e., a foil thin enough that it does not significantly perturb the flux. The activity ratio corrected for the weights of the foils, is the flux perturbation factor. Analytical methods used to treat this problem are discussed by Osborn (19) and Hanna (20), and a review of the state-of-the-art is presented in ANL-5800 (17). It is not the intent here to reiterate the discussions of the above references but to state the consensus of opinion that a systematic study of foil absorption is warranted since agreement of data and of data with theory is not good.

Commonly the flux depression is divided into two parts: (a) the self-shielding perturbation which describes the shielding of the inner layers by the outer layers of the foil and (b) the outer perturbations which describe the depletion of the neutron density in the medium surrounding the foil due to absorption by the foil. The self-shielding perturbations are functions only of the foils and since the foils used were closely identical, this factor is a constant and ignorable for relative measurements.

The outer flux pertrubations are a function of the foil and the material properties of the surrounding media. This correction must be considered since the systems under study contain three different mediums. The value by which the measured activity in water must be multiplied to yield the activity for no outer flux perturbation was computed from the results of Tittle (21) as 1.14 and from Ritchie-Eldridge and Skyrme (17) as 1.27. Meister (17) presents data for 1.2 cm radius foils in water as a function of foil thickness. Our foils had a radius of 1.26 cm. and hence Meister's results are directly applicable. Interpolation of his results yielded a factor of 1.18. Since this factor was based on measured values and since it lay between the theoretically computed values, it was used in these studies. In the interior of the cavity the factor was 1.00 in all cases.

There remained the problem of a choice of factor at or very near the boundary between the water and cavity. No guideline could be found for this problem and consequently th 1.18 factor was applied to all foils that were in the water irrespective of the proximity of the boundary. On the other hand, these questionable points were neglected in plotting the thermal flux curves and the curve that appeared to make the smoothest transition between regions was used.

Cadmium Absorption of Resonance Neutrons

The 20 mil cadmium covers effectively screen out neutrons below the "cadmium cut-off" energy of about 0.4 ev. and the indium activity obtained under such covers represents activation from resonance energy neutrons. Because the bare indium foils are activated by both thermal and resonance energy neutrons, the difference in activity of the bare and cadmium covered activities is the thermal activity. However, the cadmium not only removes the thermal neutrons but also some of the neutrons of higher energies. Consequently, the cadmium shielded foil sees fewer of the epicadmium neutrons of interest. The factor

by which the experimentally determined resonance activation must be multiplied in order to correct for the absorption of the foil resonance neutrons by the cadmium is called the cadmium correction factor, F_{CD}. This factor was obtained from the work of Tittle (21) for our case as 1.07.

APPENDIX II

DERIVATION OF THE TWO-GROUP EQUATIONS

The two group equations to be solved for the moderator region in the cavity case are

$$D_1 \nabla^2 \phi_1 - \Sigma_1 \phi_1 = 0$$

$$D_2 \nabla^2 \phi_2 - \Sigma_2 \phi_2 + p \Sigma_1 \phi_1 = 0$$

where the subscripts 1 and 2 refer to the fast and thermal groups respectively, D is the diffusion coefficient, Σ is the removal cross section in the fast group and absorption cross section in the thermal group, ϕ is the flux, and P is the resonaance escape probability. If an infinite moderator region is assumed, then the boundary conditions applied are

(1) $\lim_{r \to \infty} \phi(r) = 0$

(2) $\lim_{r \to a} - D_1 \frac{\partial \phi_1}{\partial r} = \frac{1}{4 \pi a^2}$

(3) $\lim_{r \to a} D_2 \frac{\partial \phi_2}{\partial r} = \gamma \phi_2(a)$

where a is the radius of the cavity. Conditions (1) and (2) are common diffusion theory boundary conditions. In (2) the normalization of a unit neutron source is taken. Condition (3) arises from the fact that the net current of slow neutrons must equal the absorption rate of the cavity. If the internal flux is $\theta(r)$, then the absorption rate is proportional to the volume average of θ which can be written in terms of the value of θ at $r = a$. However, in diffusion theory the flux is continuous and hence $\theta(a) = \phi_2(a)$. Therefore, the net current at the boundary is proportional to the flux at the boundary. The constant of proportionality is written as γ which yields the condition (3).

The solution of the diffusion equations in spherical geometry are of the form

$$r\phi_1 = A_1 e^{-K_1 r} + A_2 e^{K_1 r}$$

$$r\phi_2 = C_1 e^{-K_1 r} + C_2 e^{-K_2 r} + C_3 e^{K_2 r}$$

where the A's and C's are arbitrary constants and $K_1^2 = 1/\tau$, τ is the fermi age to thermal, and $K_2^2 = \Sigma_2/D_2 = 1/L^2$. The application of the boundary conditions to these expressions yields for the thermal flux

$$\phi_2(r) = \text{constant} \left[\frac{e^{-K_1(r-a)}}{r} - \beta \frac{e^{-K_2(r-a)}}{r} \right]$$

where $$\beta = \frac{\gamma a + D_2(1 + K_1 a)}{\gamma a + D_2(1 + K_2 a)}$$

The value of γ was obtained from the devlopements of Safanov as mentioned previously and is given as

$$\frac{\Sigma_2^1 a}{3} \left[1 - \frac{1}{6} (\Sigma_2^1 a)^2 \right]$$

where Σ_2^1 is the thermal absorption cross section of the interior medium. In this study, the value of Σ_2^1 used was the BF_3 value in the cavity. For the cases of an inner sphere, Σ_2^1 was computed as if the BF_3 was uniformly distributed in the cavity.

The constants used for the calculations were

$L = 2.73$ cm.

$\Sigma_2 = 0.0195/\text{cm}.$

$D_2 = 0.146$ cm.

$\tau = 54\ \text{cm}^2$

σ_a of boron = 669 barns.

σ_a of fluorine = 0

Appendix III

Tabulation of Foil Activation Data

In this appendix, the average values of the bare and cadmium covered foil activation data are tabulated. Corrections 1 through 5 as described on page 16 have been applied.

Relative Activities

Distance from Center (inches)	Figure 5 Activities of Cadmium Covered Foils		Figure 6 Bare Foils Air Filled Cavity	
1.0	466		4060	
1.5	434		-	
2.0	390		4350	
2.5	388		-	
3.0	374		4260	
3.5	356		-	
4.0	355		4080	
4.5	343		-	
5.0	362		4070	
5.5	385		-	
6.0	343		4070	
6.5	352		-	
7.0	352		4080	
7.5	341		-	
8.0	348		4020	
8.5	344		-	
9.0	347		3850	
9.5	371		-	
10.0	344		3990	
10.5	349		-	
11.0	344		3890	
11.5	358		-	
12.0	333		3900	
12.5	323		-	
13.0	313		3620	
13.5	318		-	
14.0	269		3290	
14.5	-	279*	-	3280*
15.0	-	-	2820	2870*
15.5	-	231*	-	2810*
16.0	-	-	2140	-
16.5	-	178*	-	2140*
17.0	-	-	1690	-
17.5	-	126*	-	1600*
18.0	-	-	1230	-
18.5	-	94.1*	-	1190*
19.0	-	-	-	-
19.5	-	66.6*	-	808*
20.0	-	-	-	-
20.5	-	46.9*	-	610*
21.0	-	-	-	-
21.5	-	35.7*	-	418*
22.0	-	-	-	-
22.5	-	26.2*	-	286*
23.0	-	-	-	-
23.5	-	-	-	179*
24.0	-	-	-	-
24.5	-	-	-	-
25.0	-	-	-	-
25.5	-	-	-	-

* In-water data

Relative Activities

Distance from Center (inches)	Figure 7 Bare Foils 1 atm BF_3 filling in no inner sphere system		Figure 8 Bare Foils 1 atm BF_3 filling in 12" inner sphere system	
1.0	1400		2780	
1.5	1470		3100	
2.0	1360		3000	
2.5	-		3100	
3.0	1360		3100	
3.5	-		3090	
4.0	1290		3150	
4.5	-		3160	
5.0	1310		3190	
5.5	1270		3220	
6.0	1230		3260	
6.5	-		3290	
7.0	1230		3380	
7.5	-		3360	
8.0	1210		3370	
8.5	-		3360	
9.0	1240		3380	
9.5	1220		3360	
10.0	1220		3470	
10.5	-		3350	
11.0	1190		3420	
11.5	-		3370	
12.0	1260		3350	
12.5	-		3280	
13.0	1240		3240	
13.5	1350		3100	3220*
14.0	1490		2930	-
14.5	-	2450*	2810	3160*
15.0	1650	2670*	2540	-
15.5	-	2670*	2230	2760*
16.0	1670	2460*	2060	-
16.5	-	2190*	1660	2180*
17.0	1440	1980*	-	-
17.5	1270	1800*	-	1630*
18.0	1120	1490*	-	-
18.5	-	1320*	-	1320*
19.0	804	1100*	-	-
19.5	-	918*	-	883*
20.0	628	778*	-	-
20.5	-	676*	-	611*
21.0	461	567*	-	-
21.5	373	429*	-	446*
22.0	298	398*	-	-
22.5	-	316*	-	325*
23.0	162	272*	-	-
23.5	-	217*	-	225*
24.0	75.2	163*	-	-
24.5	-	132*	-	-
25.0	-	89.4*	-	-
25.5	-	64.8*	-	-

* In-water data

Relative Activities

Distance from Center (inches)	Figure 9 Bare Foils 2 atm BF_3 filling in 12" inner sphere system		Figure 10 Bare Foils 2.5 atm BF_3 filling in 12" inner sphere system	
1.0	2170		1870	
1.5	-		-	
2.0	2470		2230	
2.5	-		-	
3.0	2370		2220	
3.5	-		-	
4.0	2520		2170	
4.5	-		-	
5.0	2540		2380	
5.5	-		-	
6.0	2740		2510	
6.5	-		-	
7.0	2830		2790	
7.5	-		-	
8.0	2850		2800	
8.5	-		-	
9.0	2930		2800	
9.5	-		-	
10.0	3000		2790	
10.5	-		-	
11.0	2890		2890	
11.5	-		-	
12.0	2940		2850	
12.5	-		-	
13.0	2840		2740	
13.5	-		-	2830*
14.0	-		-	-
14.5	-	3090*	-	3020*
15.0	-	-	-	-
15.5	-	2860*	-	2880*
16.0	-	-	-	-
16.5	-	2280*	-	2160*
17.0	-	-	-	-
17.5	-	1570*	-	1720*
18.0	-	-	-	-
18.5	-	1190*	-	1290*
19.0	-	-	-	-
19.5	-	834*	-	856*
20.0	-	-	-	-
20.5	-	605*	-	638*
21.0	-	-	-	-
21.5	-	473*	-	448*
22.0	-	-	-	-
22.5	-	337*	-	302*
23.0	-	-	-	-
23.5	-	-	-	216*
24.0	-	-	-	-

* In-water data

Relative Activities

Distance from Center (inches)	Figure 11 Bare Foils 1 atm BF_3 filling in 9" inner sphere system		Figure 12 Bare Foils 2 atm BF_3 filling in 9" inner sphere system
1.0	3210		2530
1.5	-		-
2.0	3370		2920
2.5	-		-
3.0	3480		2960
3.5	-		-
4.0	3550		3180
4.5	-		-
5.0	3560		3340
5.5	-		-
6.0	3670		3360
6.5	-		-
7.0	3700		3440
7.5	-		-
8.0	3630		3440
8.5	-		-
9.0	3630		3370
9.5	-		-
10.0	3550		3450
10.5	-		-
11.0	3640		3350
11.5	-		-
12.0	3460		3340
12.5	-		-
13.0	3320		3210
13.5	-	3510*	-
14.0	3130	-	3060
14.5	-	3280*	-
15.0	2730	-	2500
15.5	-	2880*	-
16.0	2220	-	2130
16.5	-	2310*	-
17.0	1690	-	1600
17.5	-	1630*	-
18.0	-	-	1160
18.5	-	1180*	-
19.0	-	-	859
19.5	-	900*	-
20.0	-	-	652
20.5	-	610*	-
21.0	-	-	448
21.5	-	431*	-
22.0	-	-	314
22.5	-	310*	-
23.0	-	-	179
23.5	-	-	-
24.0	-	-	69.4

* In-water data

Relative Activities

Figure 13
Bare Foils
3 atm BF_3 filling in
9" inner sphere system

Distance from Center (inches)	
1.0	2350
1.5	-
2.0	2560
2.5	-
3.0	2780
3.5	-
4.0	2980
4.5	-
5.0	3100
5.5	-
6.0	3370
6.5	-
7.0	3280
7.5	-
8.0	3380
8.5	-
9.0	3300
9.5	-
10.0	3270
10.5	-
11.0	3220
11.5	-
12.0	3250
12.5	-
13.0	3030
13.5	-
14.0	2830
14.5	-
15.0	2480
15.5	-
16.0	2100
16.5	-
17.0	1590
17.5	-
18.0	1190
18.5	-
19.0	874
19.5	-
20.0	676
20.5	-
21.0	475
21.5	-
22.0	-
22.5	-
23.0	-
23.5	-
24.0	-

REFERENCES

1. Baron, S., "Gaseous Fuel Reactor," Nucleonics, 16, No. 8, pp. 128, 130-133, August 1958.

2. Grey, J., "Gaseous Core Nuclear Rockets," Astronautics, 4, No. 10, pp. 23-5, 110-112, October 1959.

3. Rom, F., "Advanced Reactor Concepts for Nuclear Propulsion," Astronautics, 4, No. 10, pp. 20-2, 46-50, October 1959.

4. Meghreblian, R.V., "Gaseous Fission Reactors for Spacecraft Propulsion," J.P.L. Technical Report 32,42, July 1960.

5. Meghreblian, R.V., "Gaseous Fission Reactors for Booster Propulsion," J.P.L. Technical Report 32-56, March 1961.

6. Meghreblian, R.V., "Gaseous Propulsion Reactors," Nucleonics, 19, No. 4, pp. 95-99, April 1961.

7. Weinstein, H. and Ragsdale, R., "A Coaxial Flow Reactor - A Gaseous Nuclear-Rocket Concept," Preprint 1518-60, Am. Rocket Soc., 1960.

8. Nelson, S.T., "The Plasma Core Reactor," Preprint 1734-61, Am. Rocket Soc., Inc., 1961.

9. Bell, George I., "Calculations of the Critical Mass of UF_6 as a Gaseous Core with Reflectors of D_2O, Be, and C," Low Alamos Report LA 1874, February 1955.

10. Safanov, George, "Externally Moderated Reactors," Reactor Physics paper 625, Proceedings of the Second United Nations International Conference on Peaceful Uses of Atomic Energy (Geneva), 1958. Also, Rand Corporation Research Memorandum, R-316, July 1957.

11. Ragsdale, R.G. and Hyland, R.E., "Some Nuclear Calculations of U^{235} - D_2O Gaseous-Core Cavity Reactors," NASA Technical Note D-475, Lewis Research Center, Cleveland, Ohio, October 1961.

12. Hyland, R.E., Ragsdale, R.G. and Gunn, E.J., "Two-Dimensional Criticality Calculations of Gaseous Core Cylindrical Cavity Reactors," NASA TN D-1575, (1963).

13. Plunkett, T.F. and Holl, R.J., "Nuclear Analysis of Gaseous Core Reactors," Report SM-44041, Douglas Aircraft Company, Inc. May, 1963.

14. Mills, C.B., "Reflector Moderated Reactors," Nuc. Sci. and Eng., 13, 301-305, 1962.

15. Paxton, H.C. and Orndoff, J.D., "Measurements on Cavity Critical Assembly," Group N-2 Progress Report, Los Alamos Scientific Lab, Oct. 21-Nov. 20, 1960.

16. Fox, T.A., Shook, D.F., Mueller, R.A. and Fieno, D., "Experimental Neutron Flux Distributions in a Graphite Assembly with an Internal Cavity," NASA Technical Note, D-1460, October, 1962.

17. Reactor Physics Constants, Section 9, ANL-5800, July, 1963.

18. Hollander, J.M., Perlman, I., and Seaborg, G.T., "Table of Isotopes," Reactor Handbook, Vol 1, Physics, U.S.A.E.C., 1955.

19. Osborn, R.K., "A Discussion of Theoretical Analyses of Probe-Induced Thermal Flux Perturbations," Nuc. Sci and Eng., 15, 245, 1963.

20. Hanna, G.C., "The Neutron Flux Perturbation Due to an Absorbing Foil; A Comparison of Theories and Experiments," Nuc. Sci. and Eng., 15, 325, 1963.

21. Tittle, C.W., Nucleonics, 9 (1), 1951.

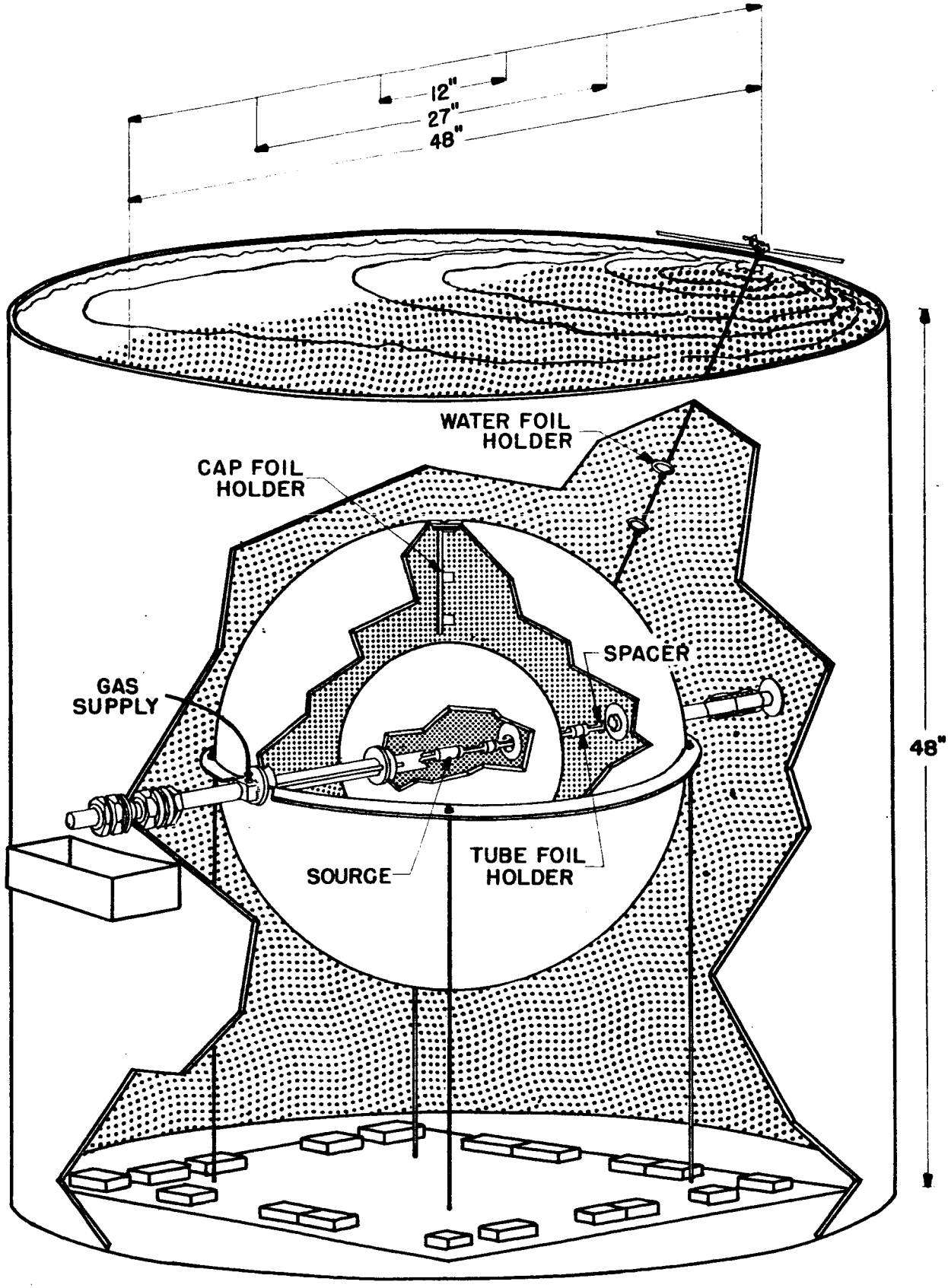

FIGURE I— PICTORIAL OF EXPERIMENTAL ASSEMBLY

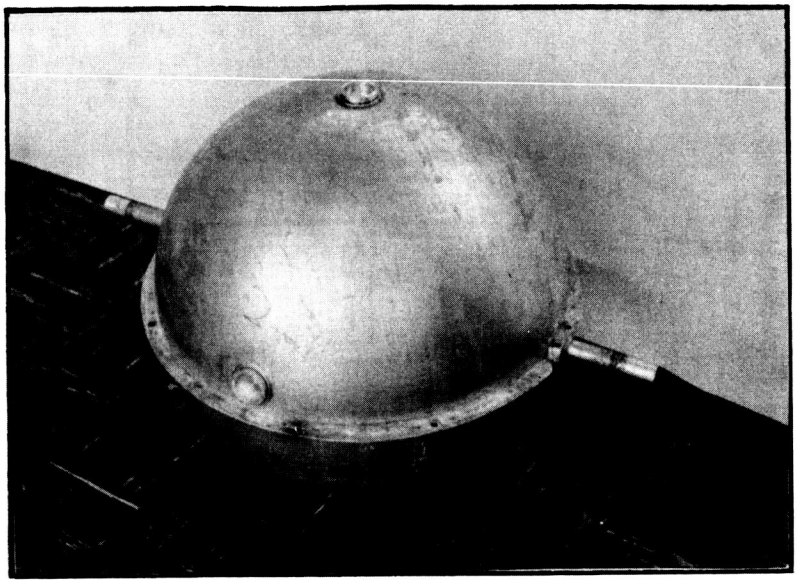

Figure 2 - Spherical cavity assembly showing the thru-tube and ports.

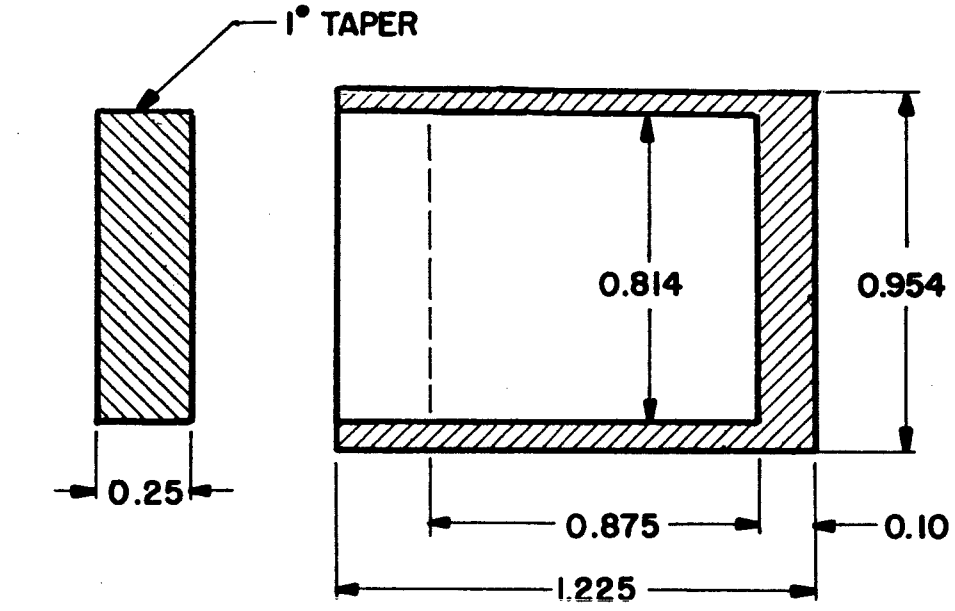

INNER CONTAINER–TANTALUM

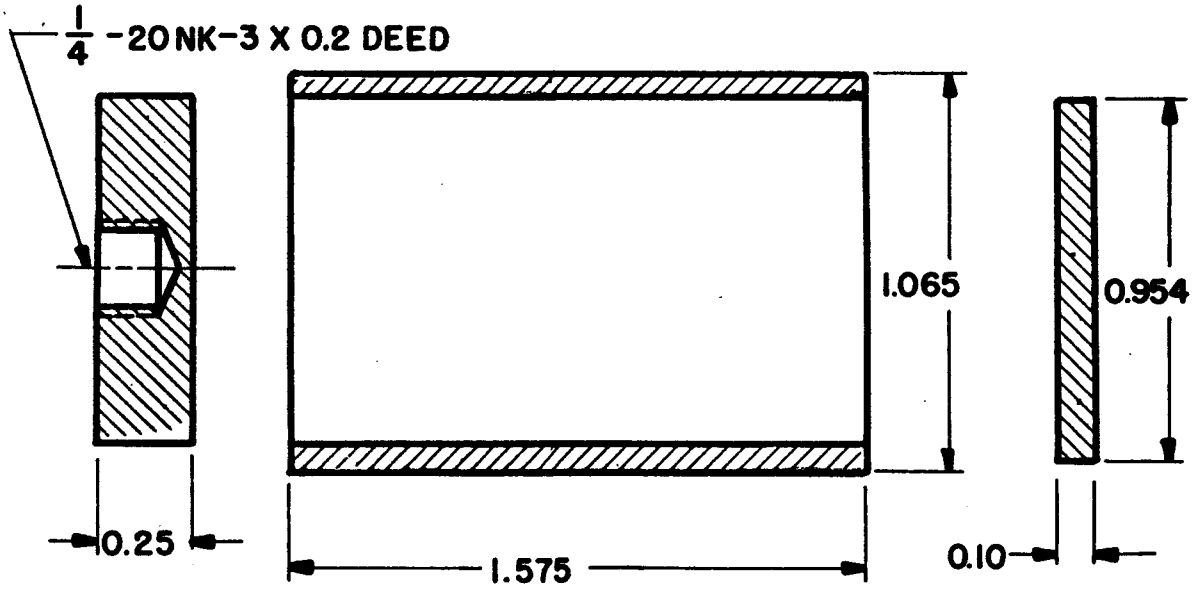

OUTER CONTAINER–304 STAINLESS STEEL

Figure 3 - Plutonium-beryllium neutron source description

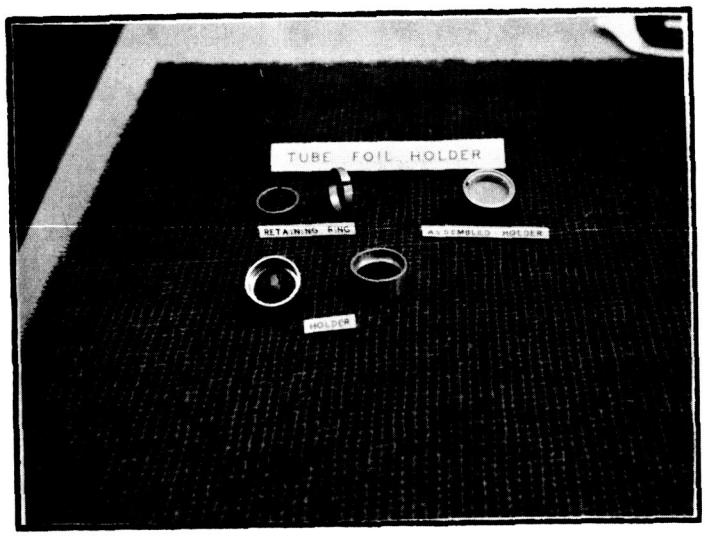

(a)

(b)

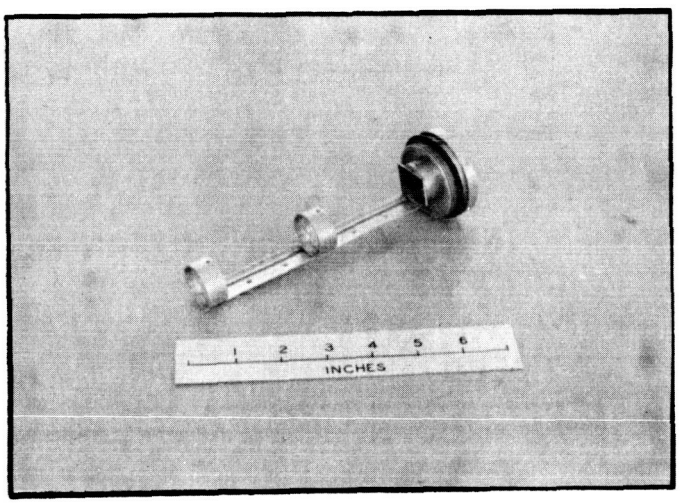

(c)

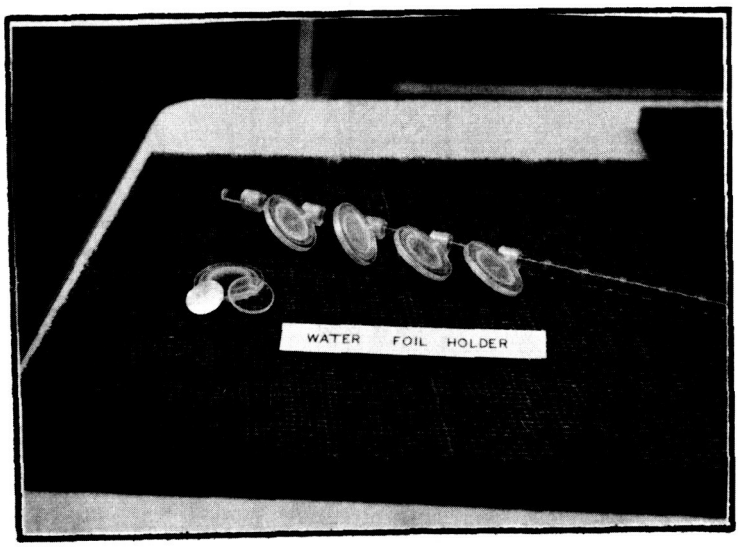

Figure 4 - Foil holders: (a) Thru-tube holder, (b) Port assembly holder, (c) Water holder

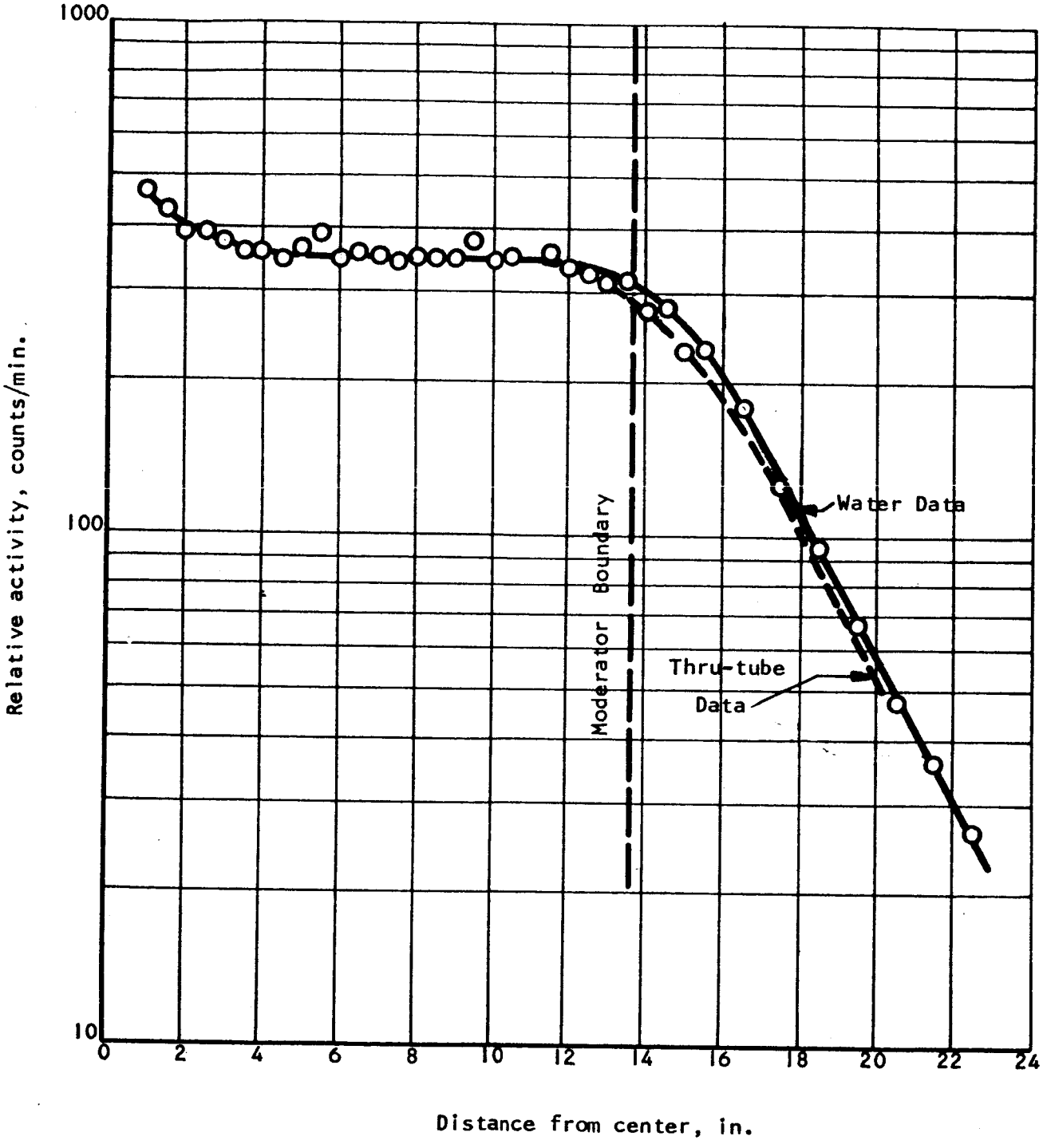

Figure 5 - Indium foil activations for cadmium covered foils.

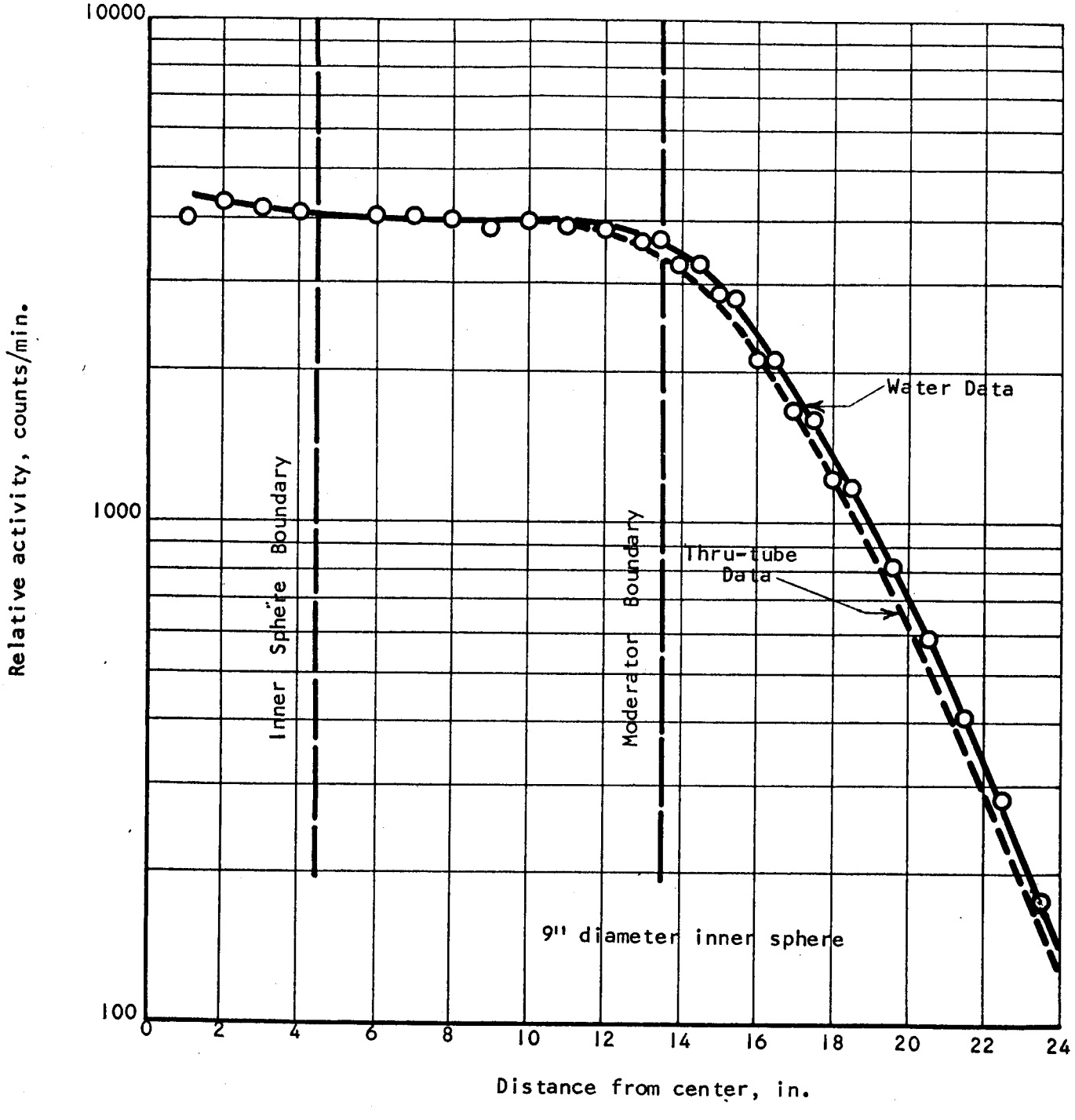

Figure 6 - Indium foil activations for bare foils for air filled cavity.

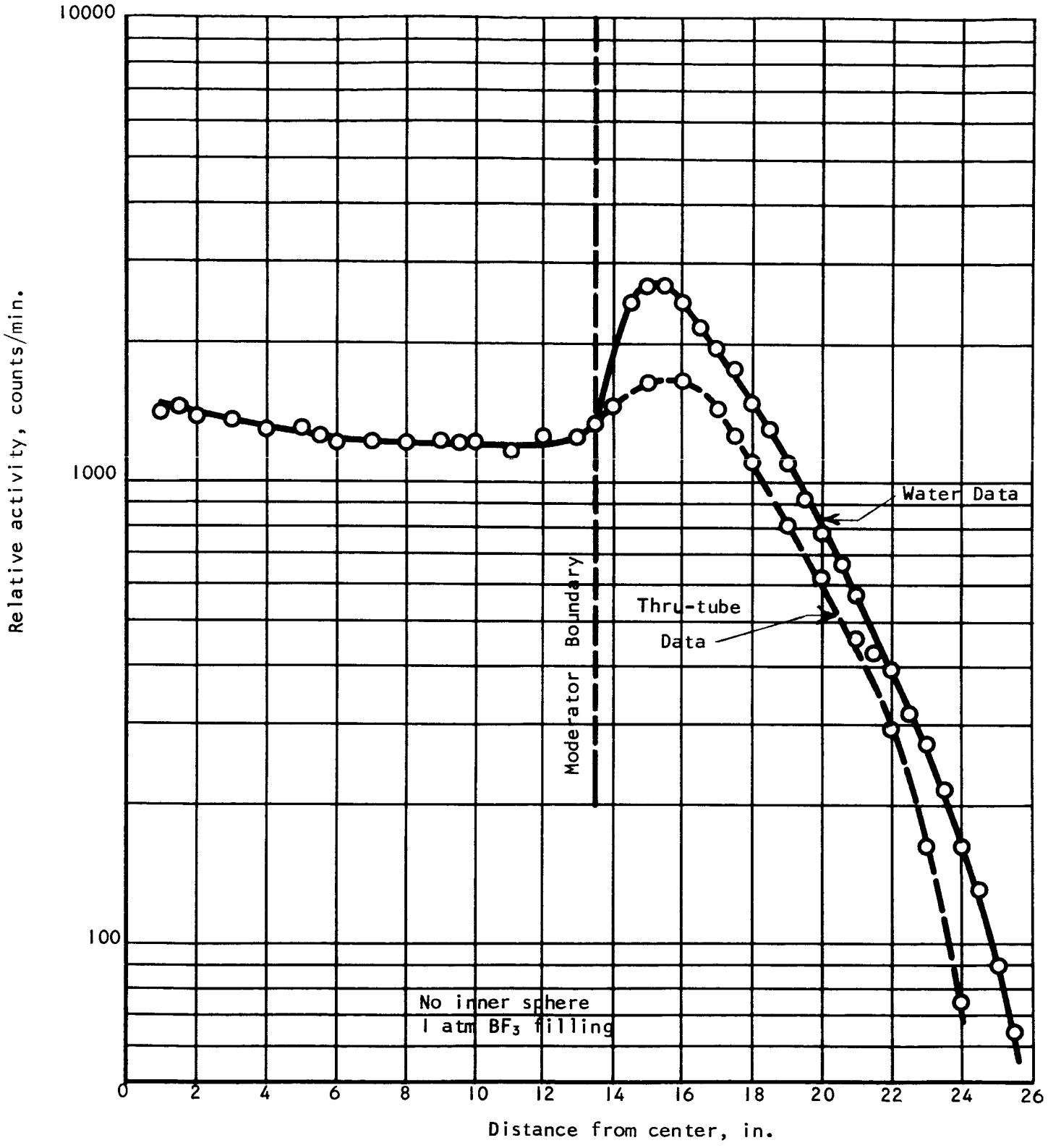

Figure 7 - Indium foil activations for bare foils for no inner sphere system with 1 atmosphere BF_3 filling.

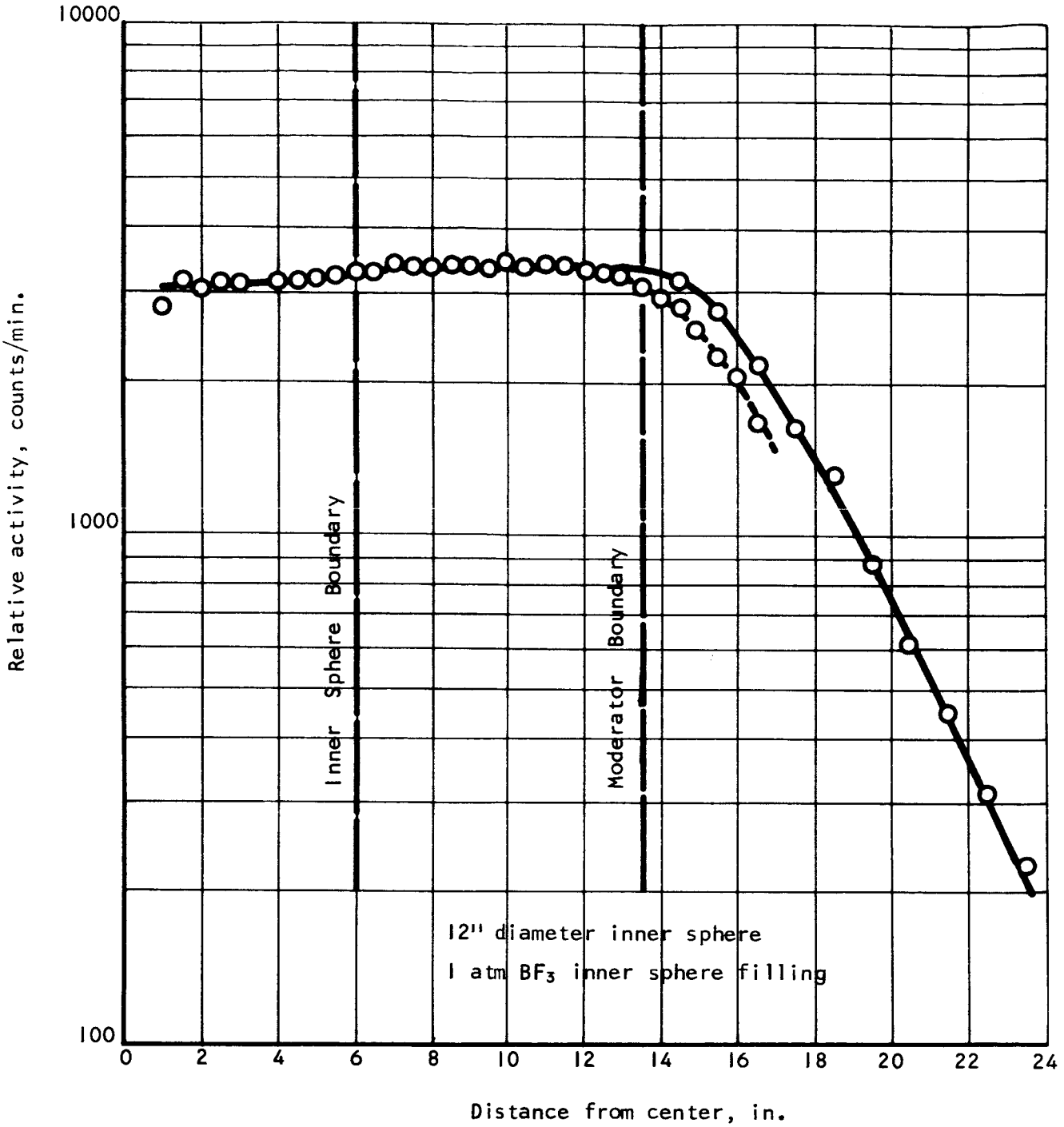

Figure 8 - Indium foil activations for bare foils for a 12 inch inner sphere system with 1 atmosphere BF_3 filling.

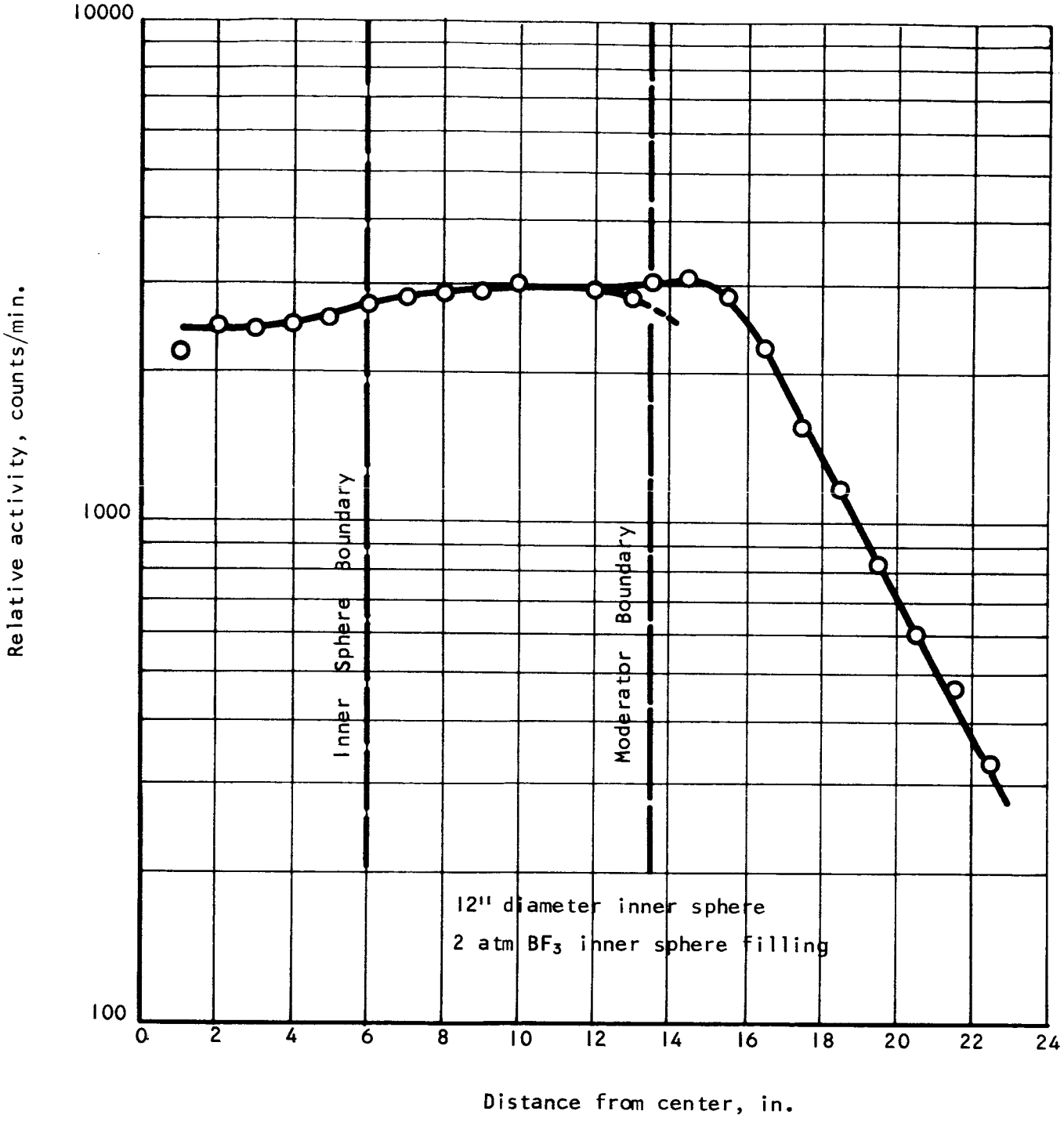

Figure 9 - Indium foil activations for bare foils for a 12 inch inner sphere system with 2 atmospheres BF_3 filling.

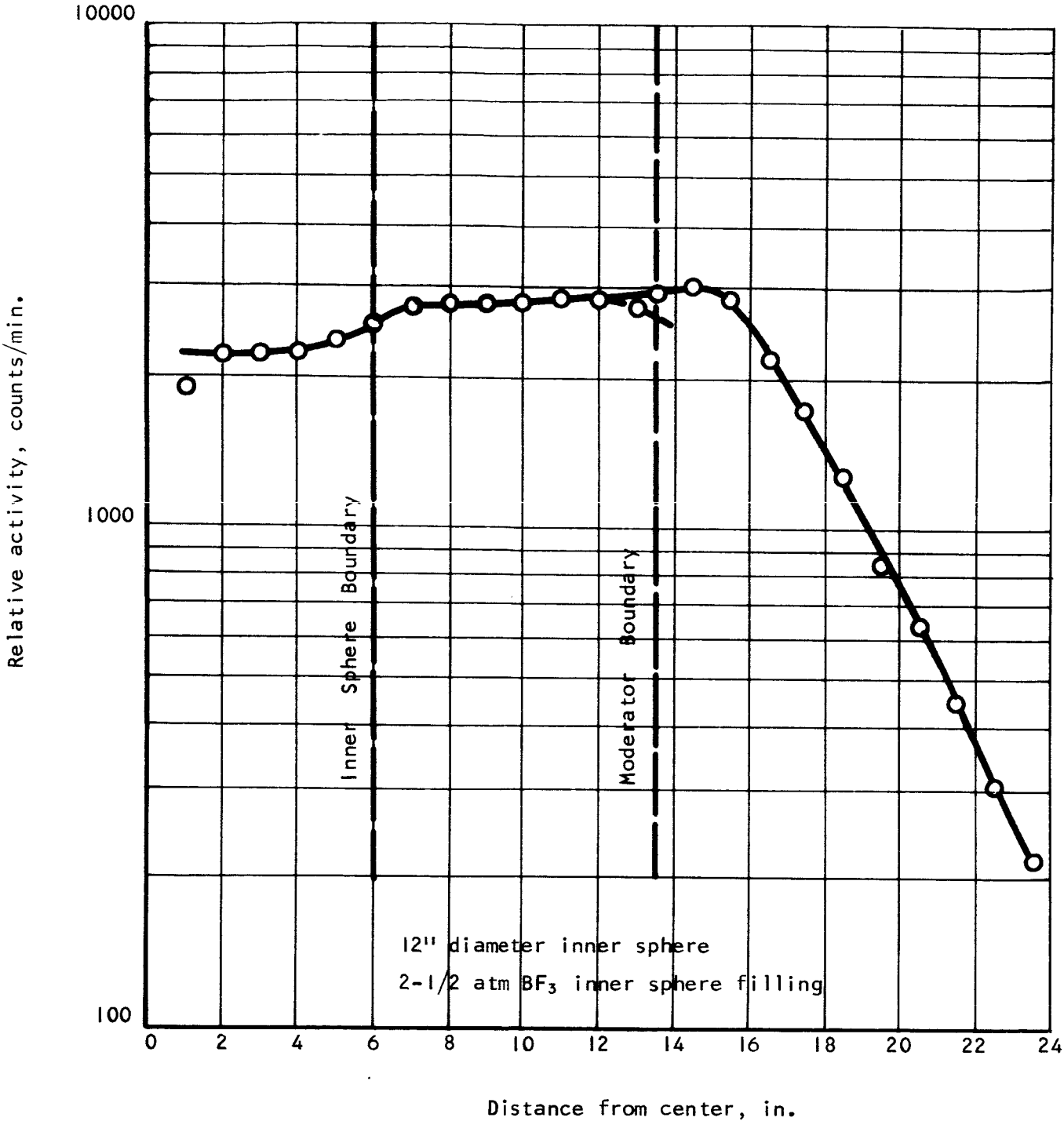

Figure 10 - Indium foil activations for bare foils for a 12 inch inner sphere system with 2.5 atmospheres BF_3 filling.

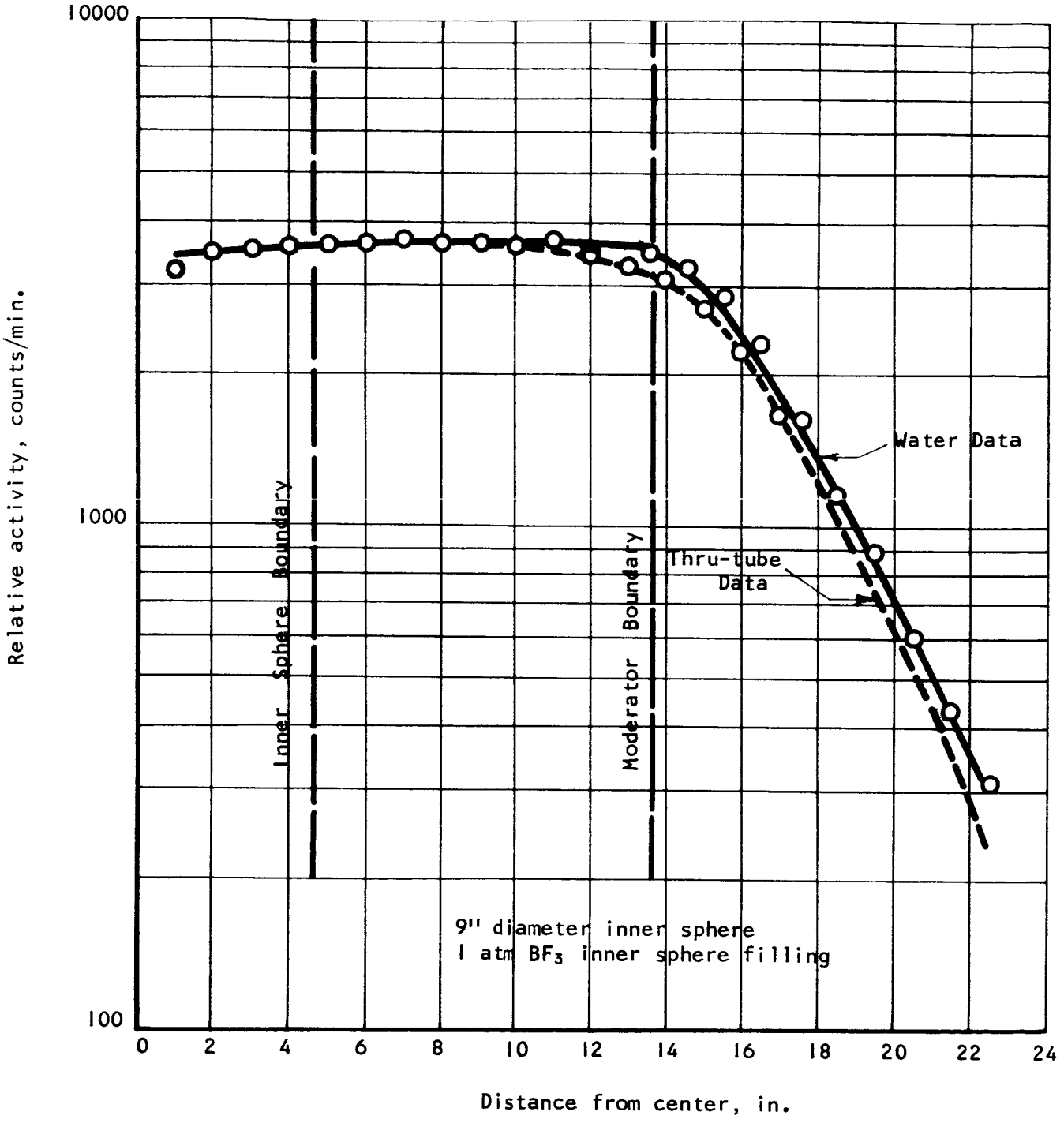

Figure II - Indium foil activations for bare foils for a 9 inch inner sphere system with 1 atmosphere BF_3 filling.

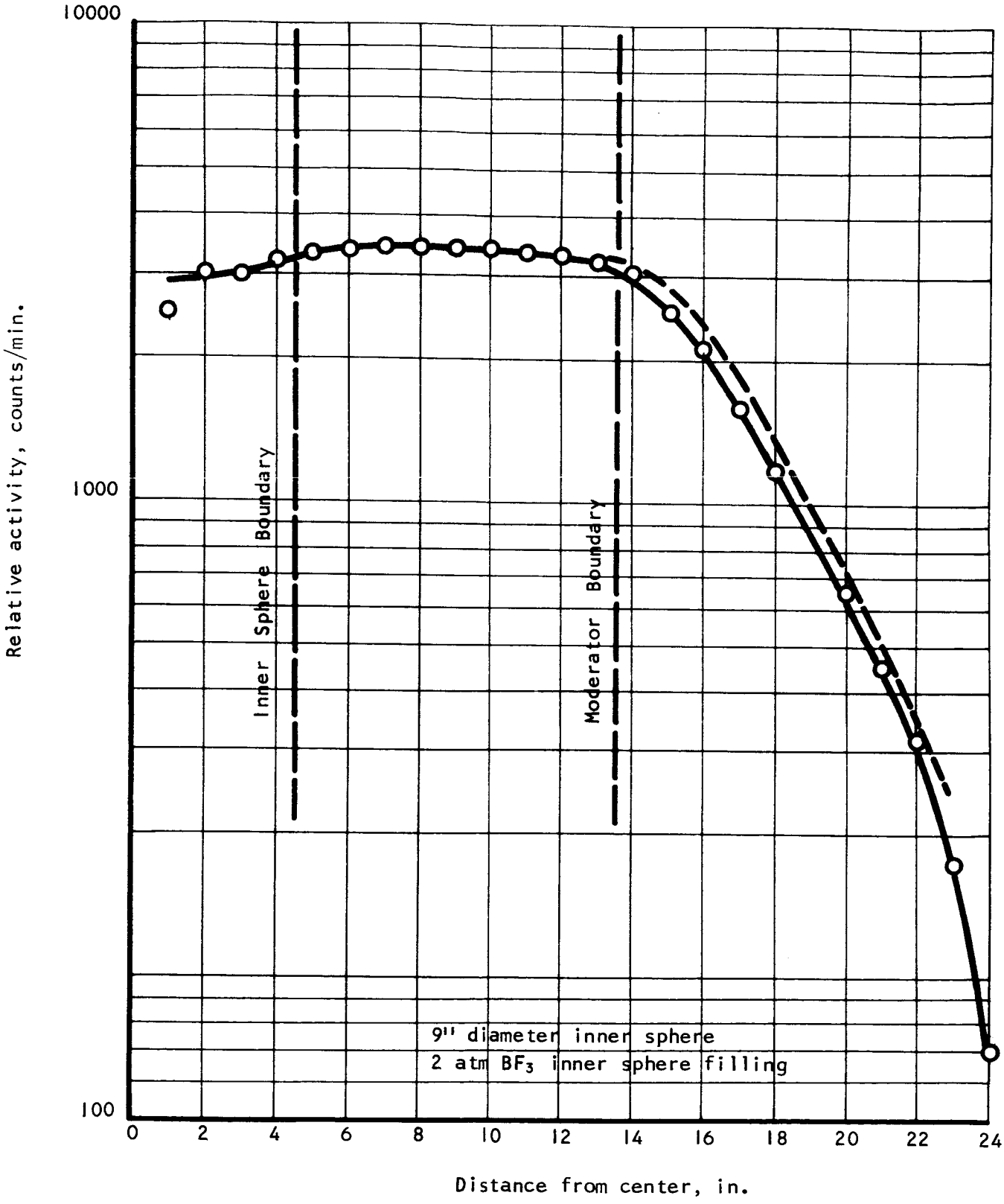

Figure 12 - Indium foil activations for bare foils for a 9 inch inner sphere system with 2 atmospheres BF_3 filling.

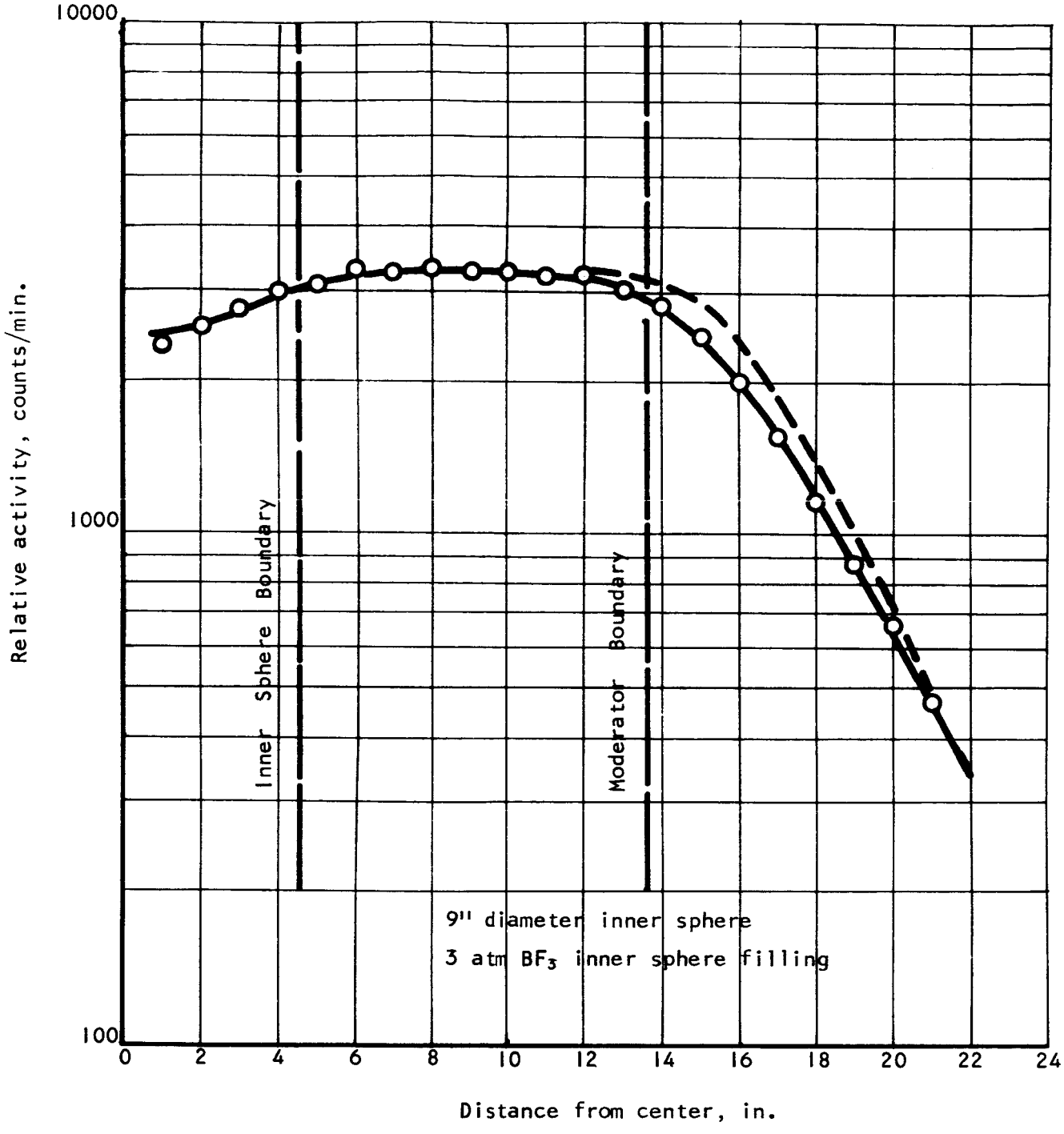

Figure 13 - Indium foil activations for bare foils for a 9 inch inner sphere system with 3 atmospheres BF_3 filling.

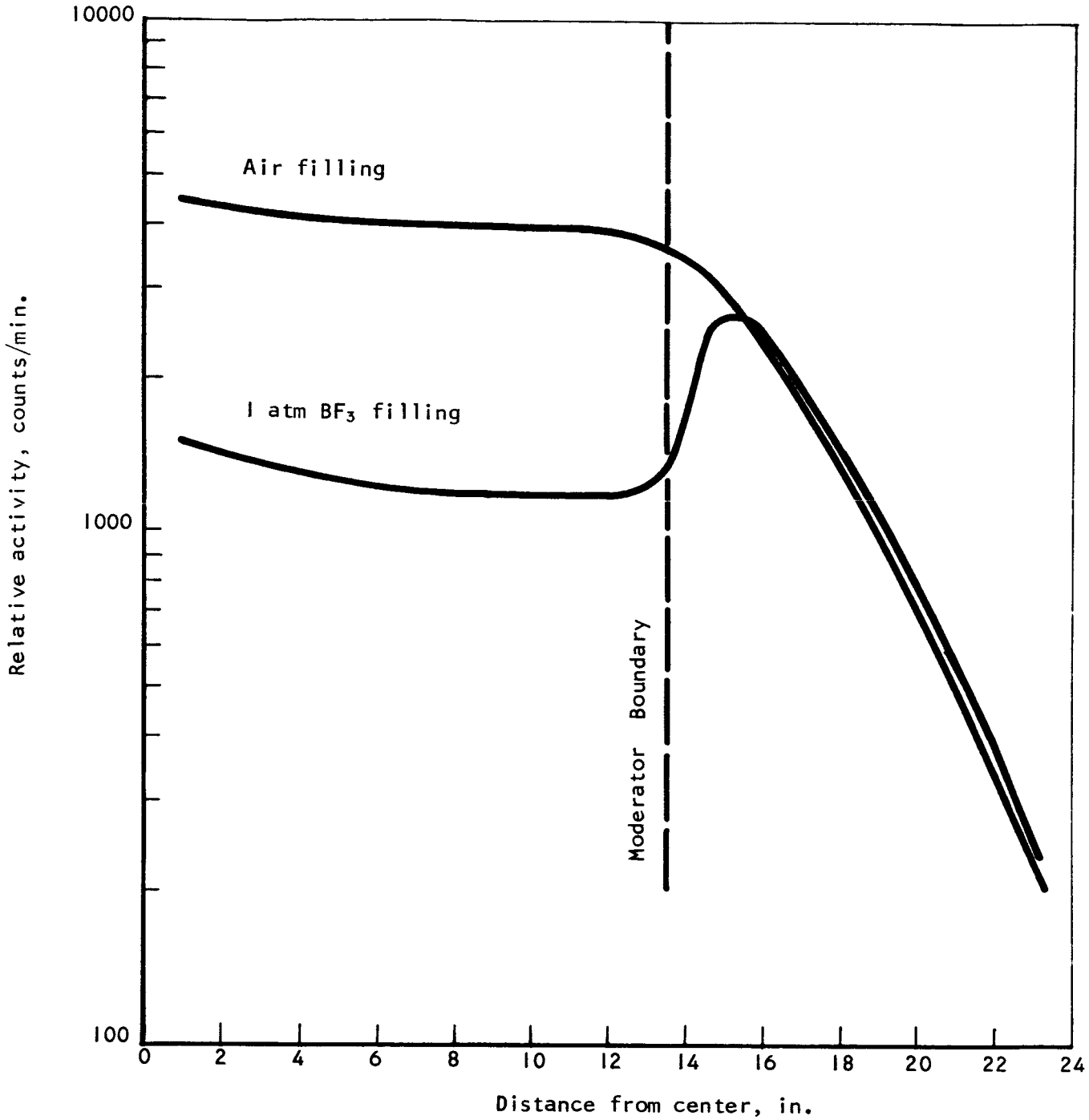

Figure 14 - Comparison of indium foil activations for bare foils in the single sphere system with air and 1 atmosphere BF_3 fillings.

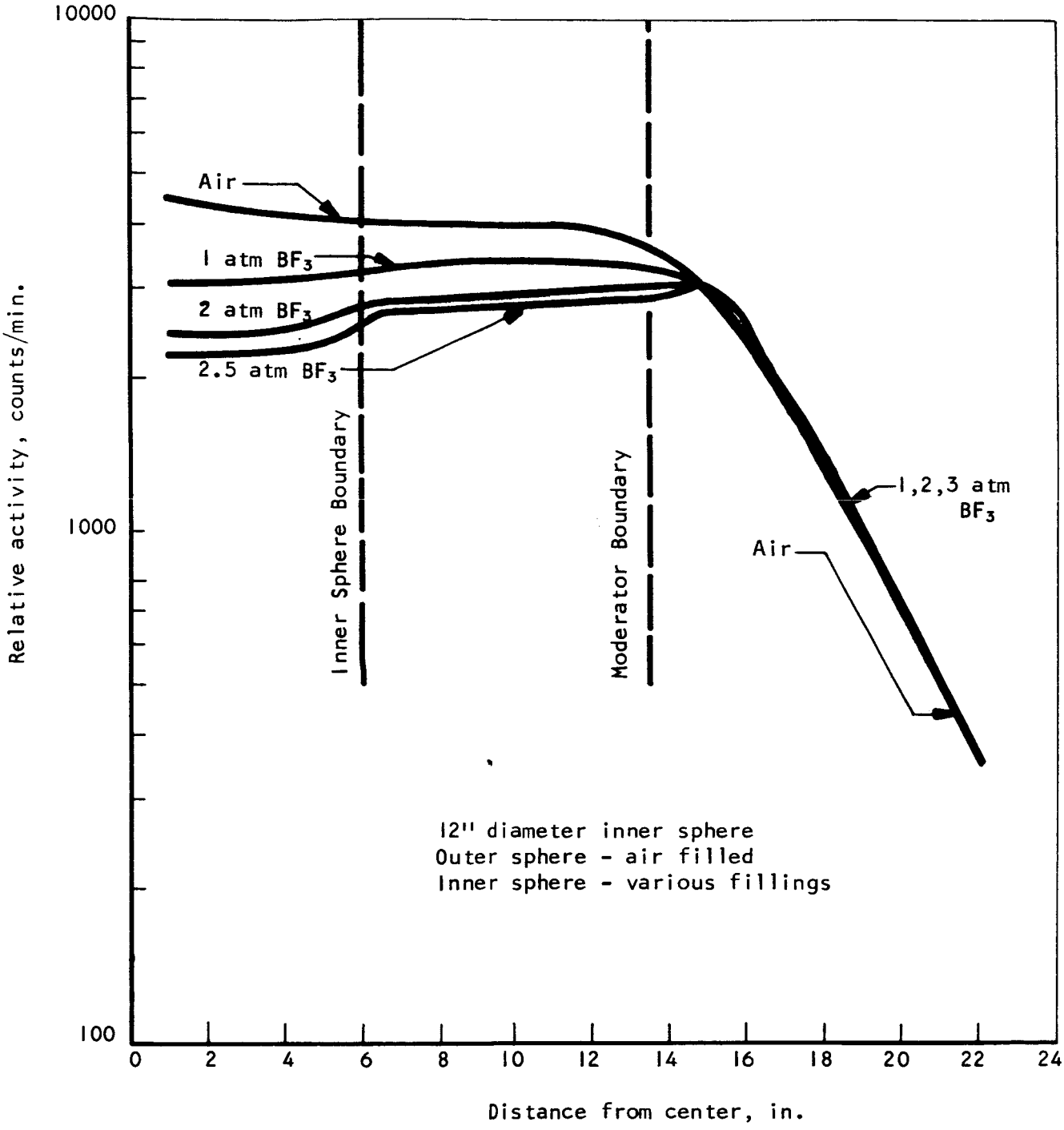

Figure 15 - Comparison of indium foil activations for bare foils in the 12 inch concentric sphere system for various inner sphere fillings.

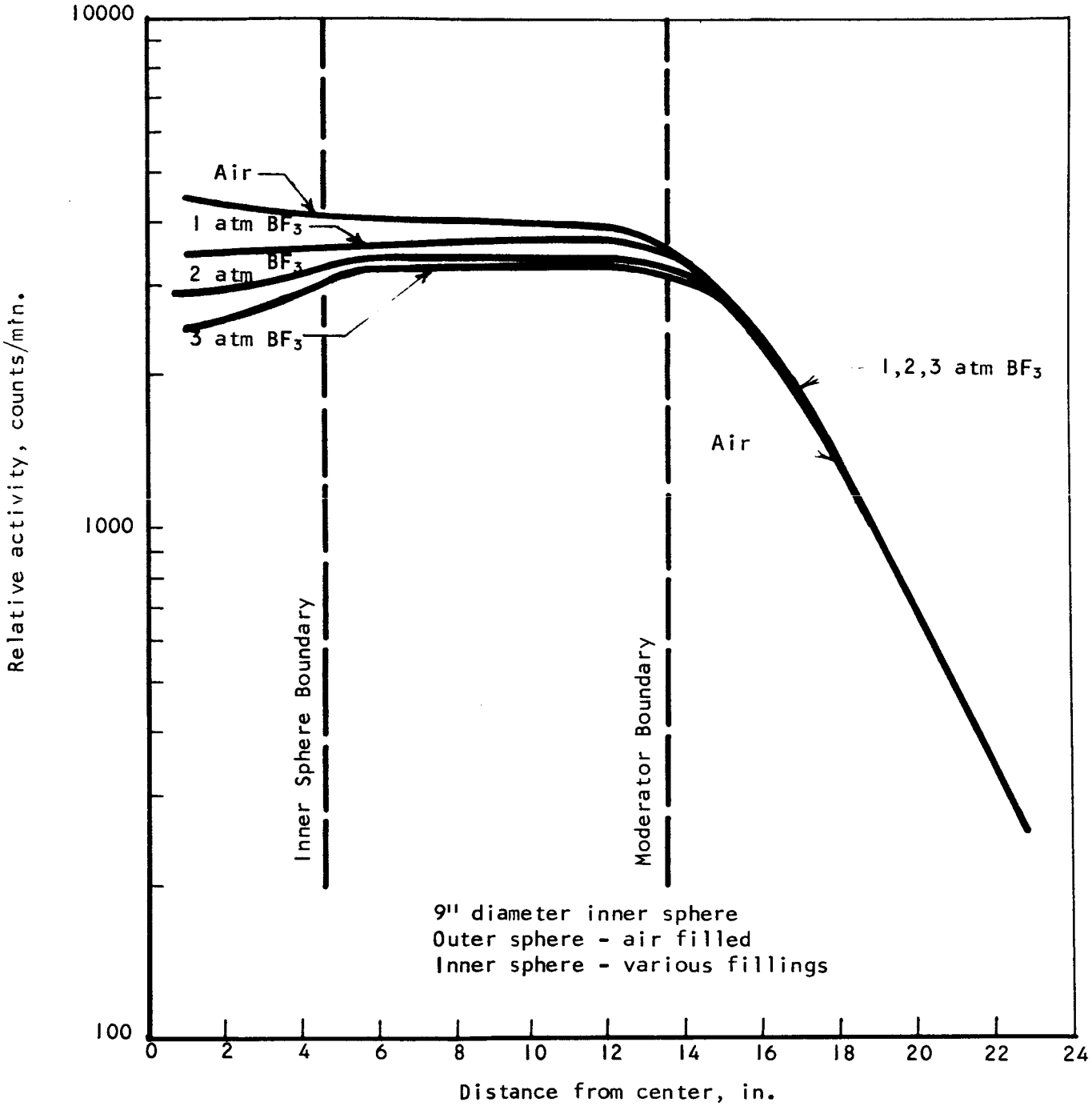

Figure 16 - Comparison of indium foil activations for bare foils in the 9 inch concentric sphere system for various inner sphere fillings.

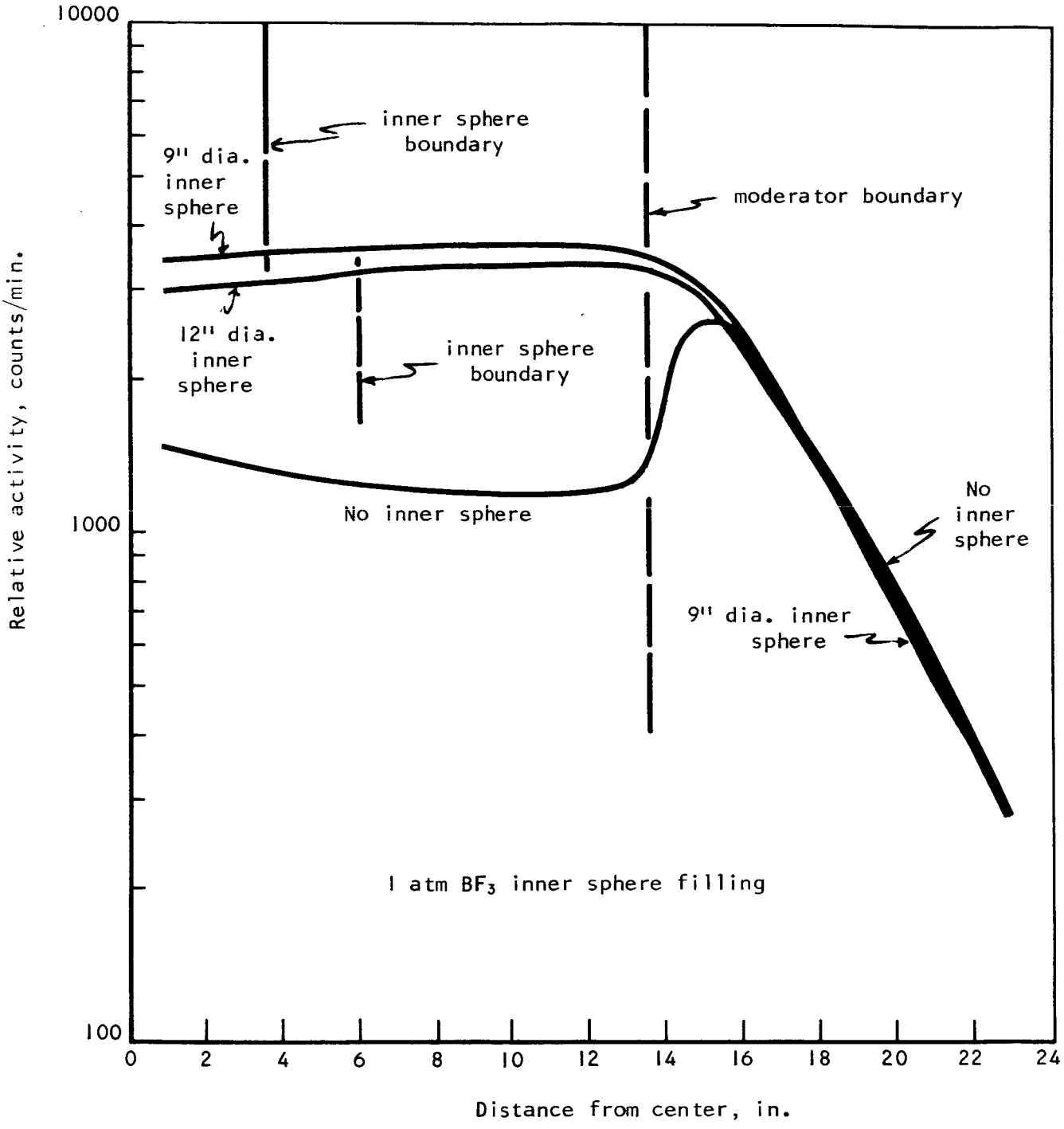

Figure 17 - Comparison of indium foil activations for bare foils for the three sphere systems with 1 atmosphere BF_3 filling.

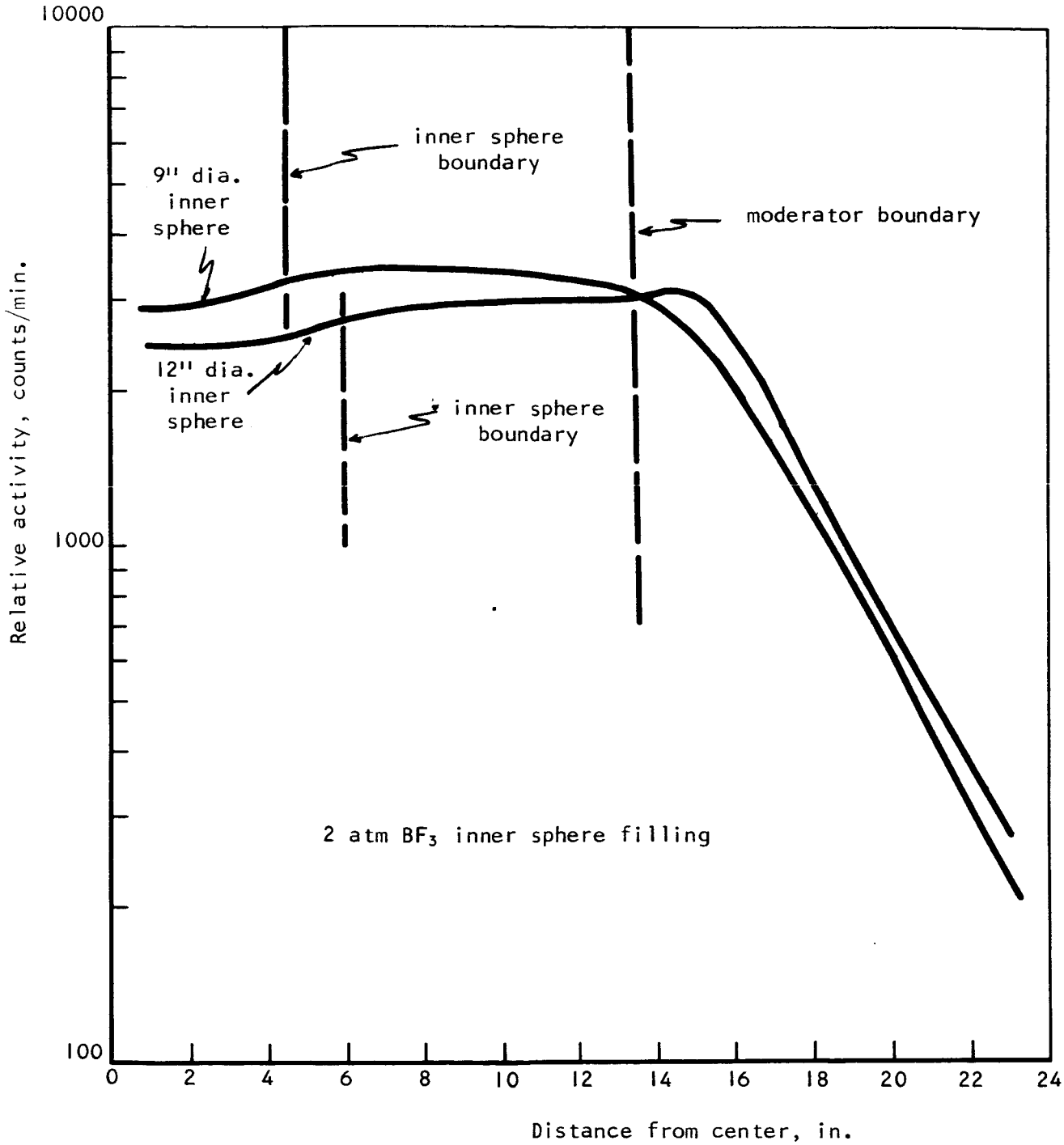

Figure 18 - Comparison of indium foil activations for bare foils for the 9 and 12 inch inner sphere systems with 2 atmospheres of BF_3 filling.

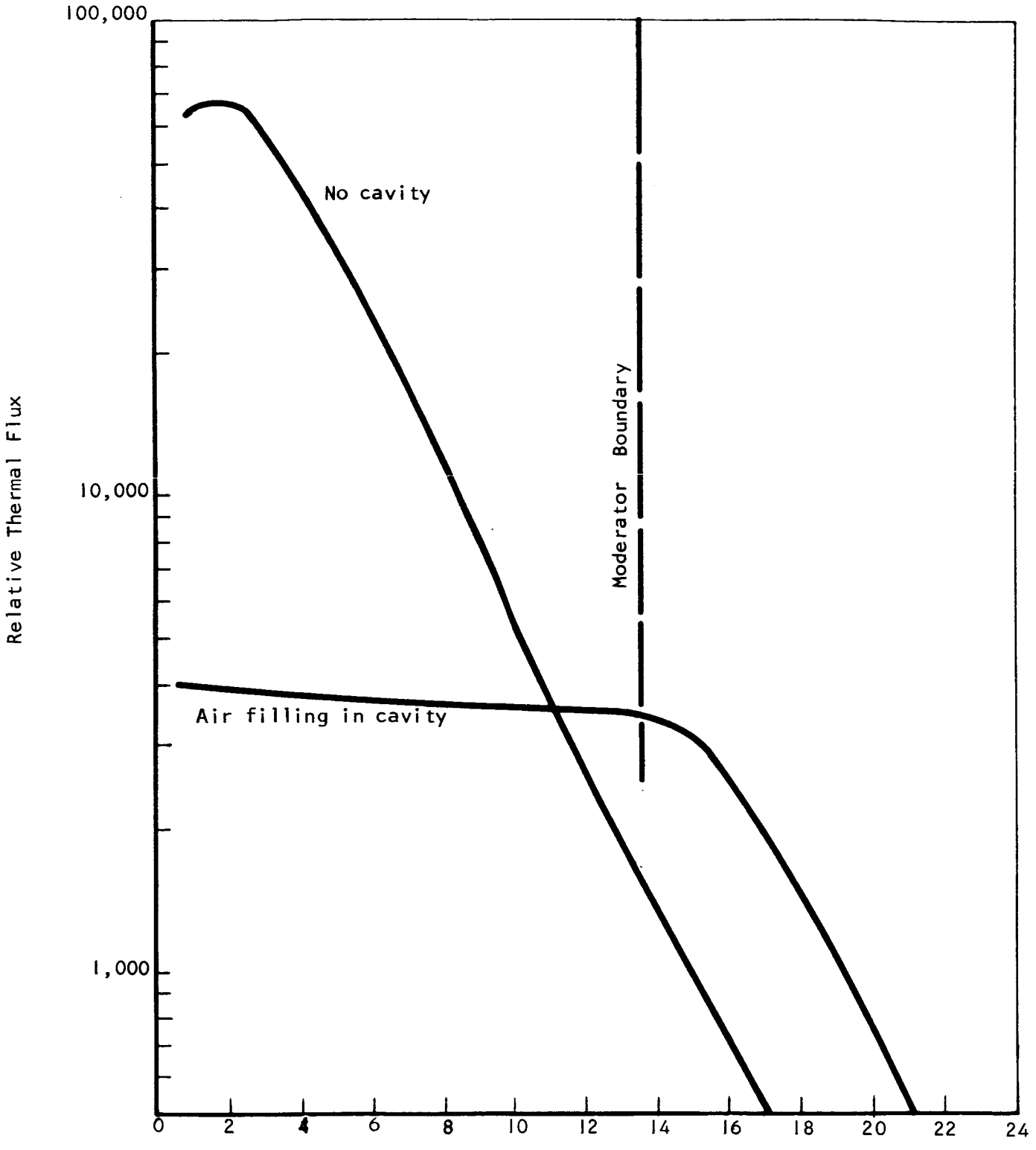

Figure 19 - Comparison of thermal flux for the cases of no cavity and air filled cavity.

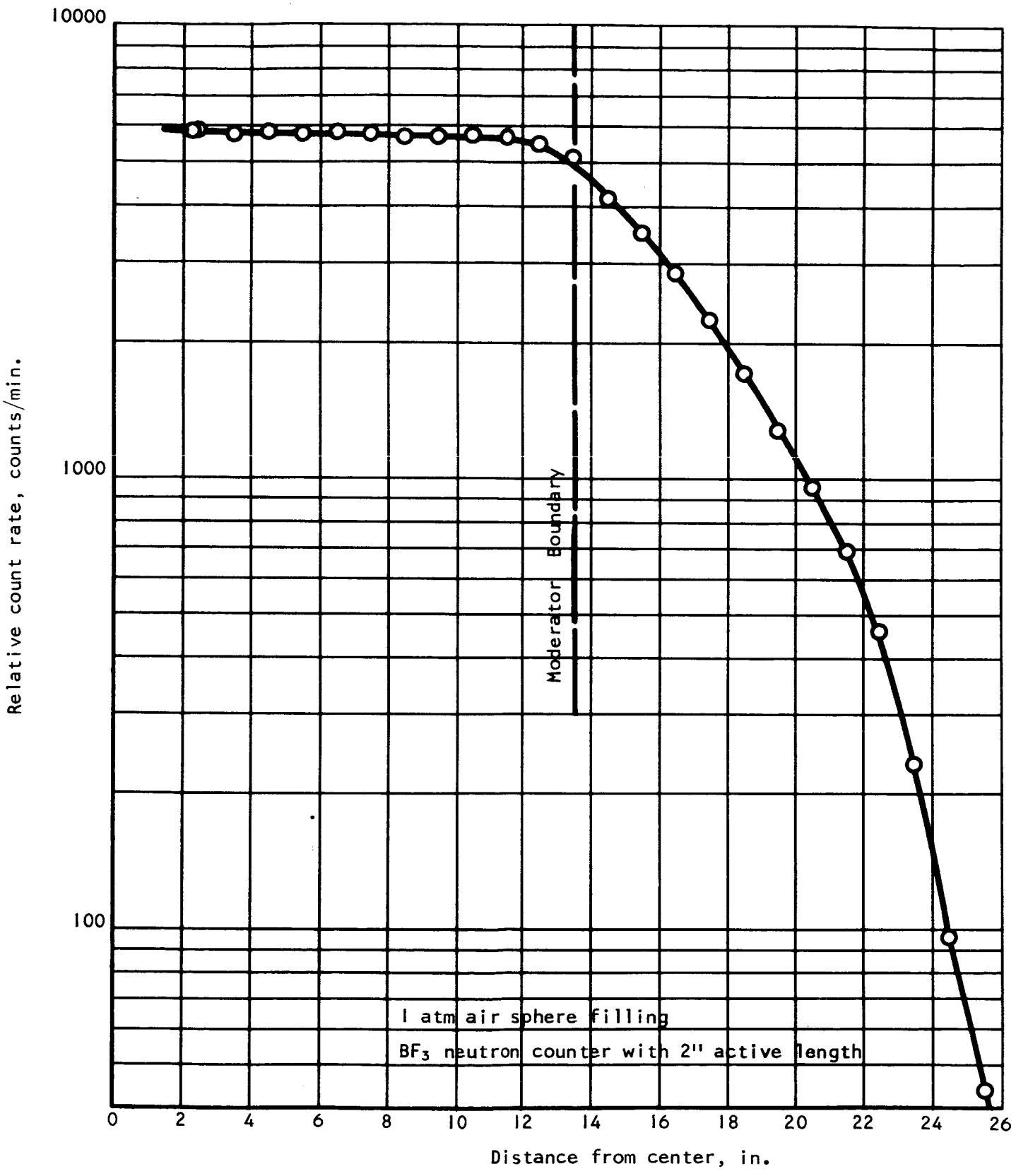

Figure 20 - BF_3 neutron counter data for the air filled cavity.

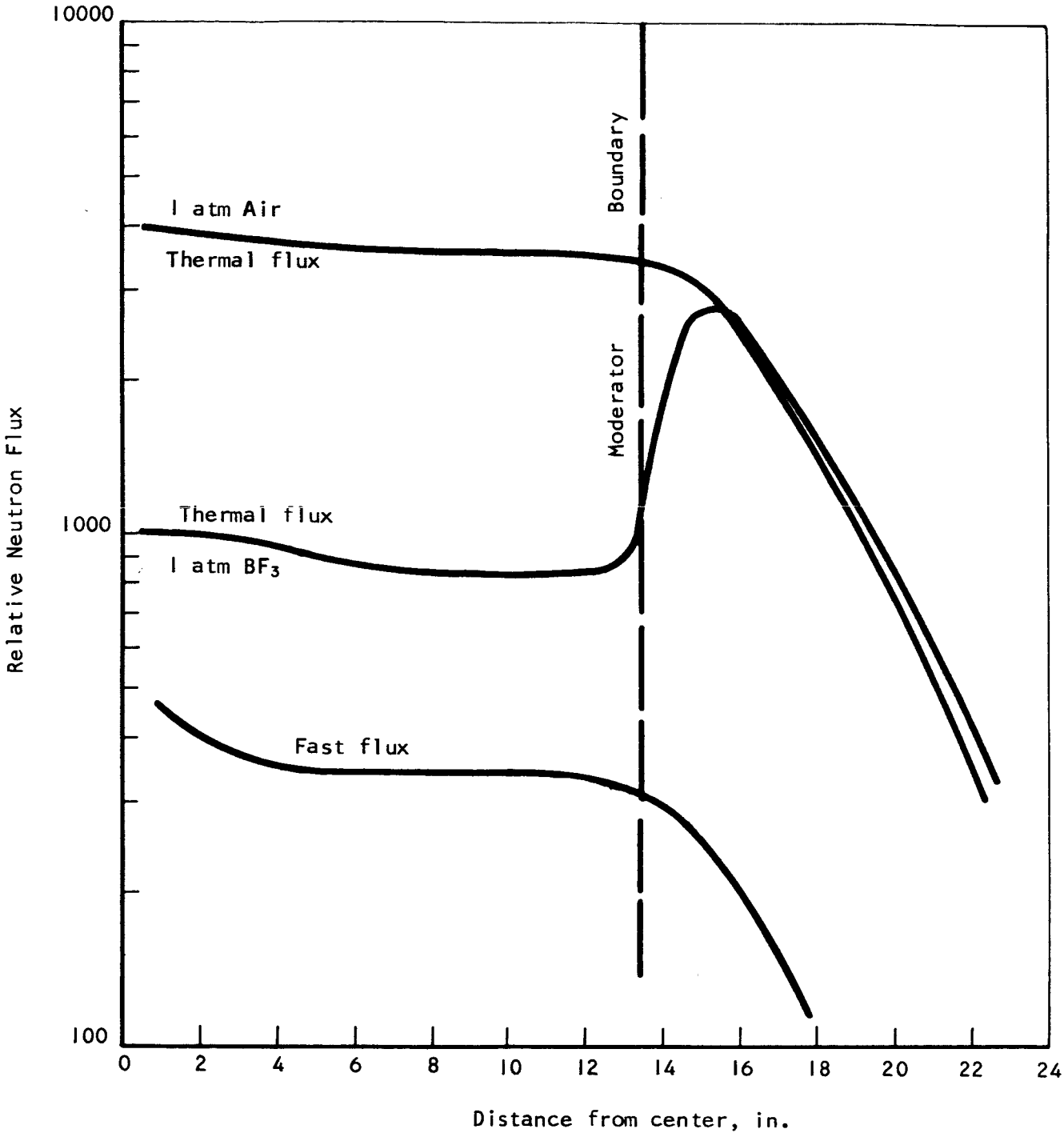

Figure 21 - Comparison of thermal neutron flux and fast flux for the single sphere system with air and 1 atmosphere BF_3 filling.

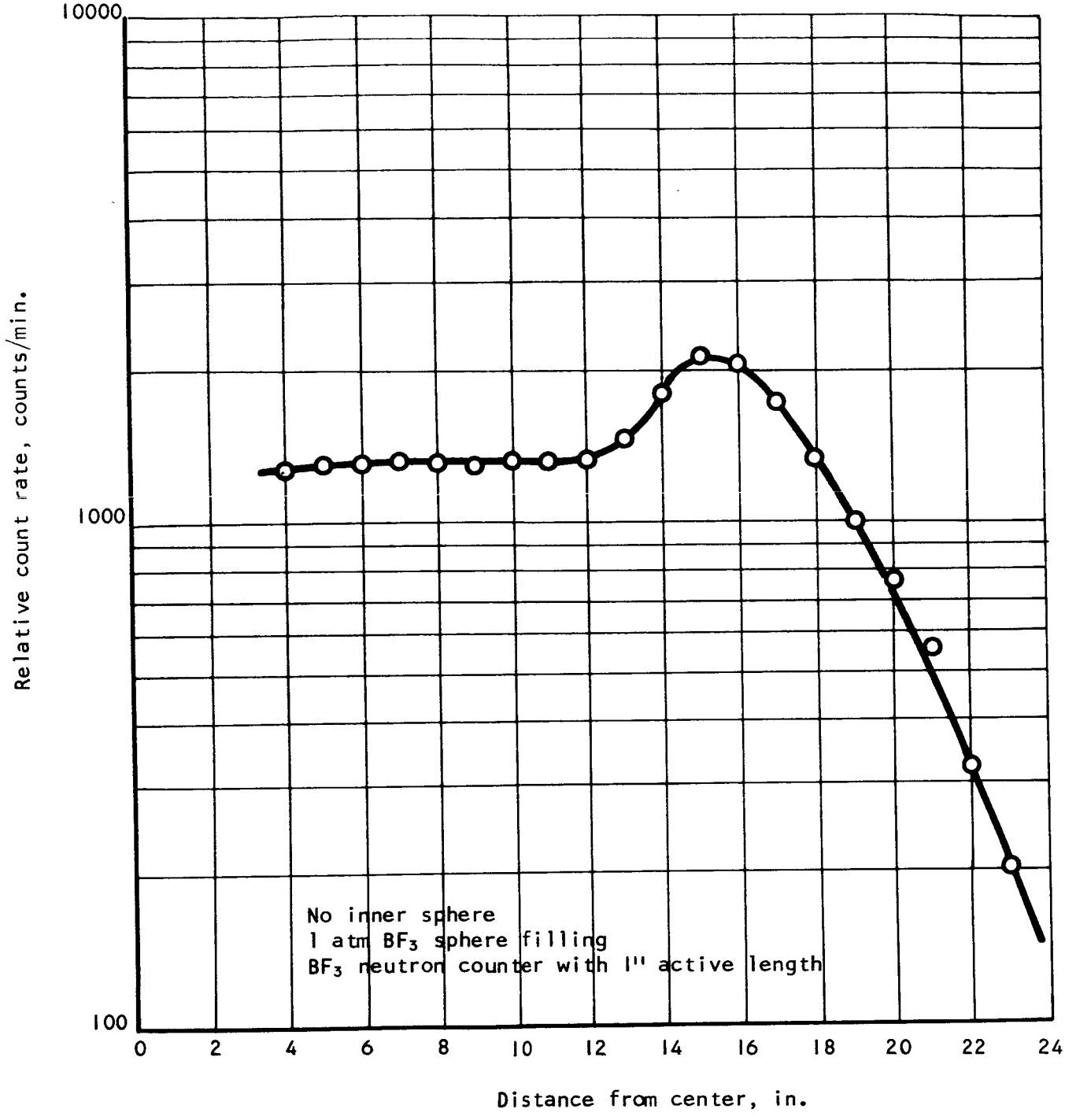

Figure 22 - BF_3 neutron counter data for the single sphere case with 1 atmosphere BF_3 filling.

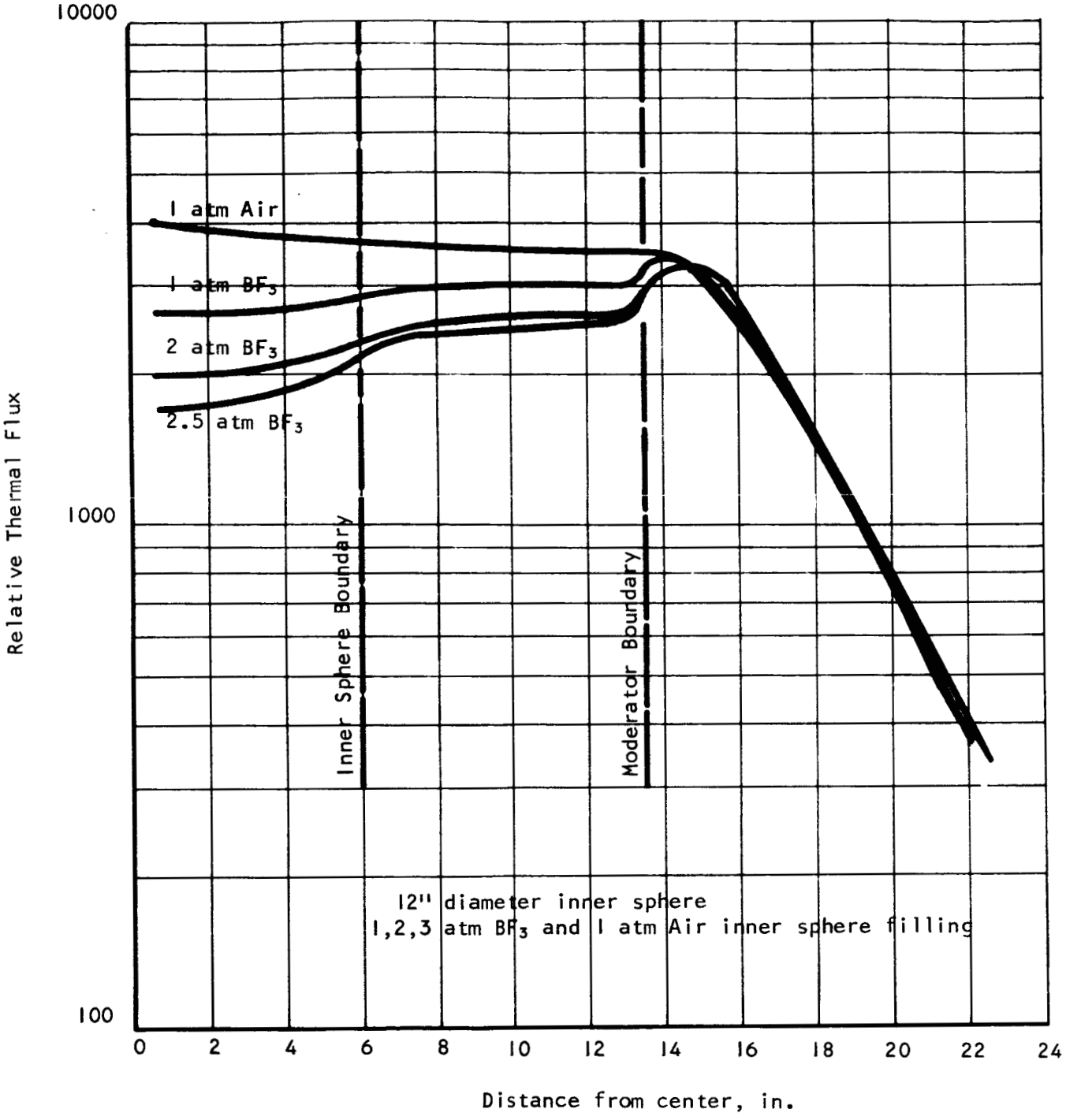

Figure 23 - Comparison of thermal flux for the 12 inch inner sphere system with various fillings.

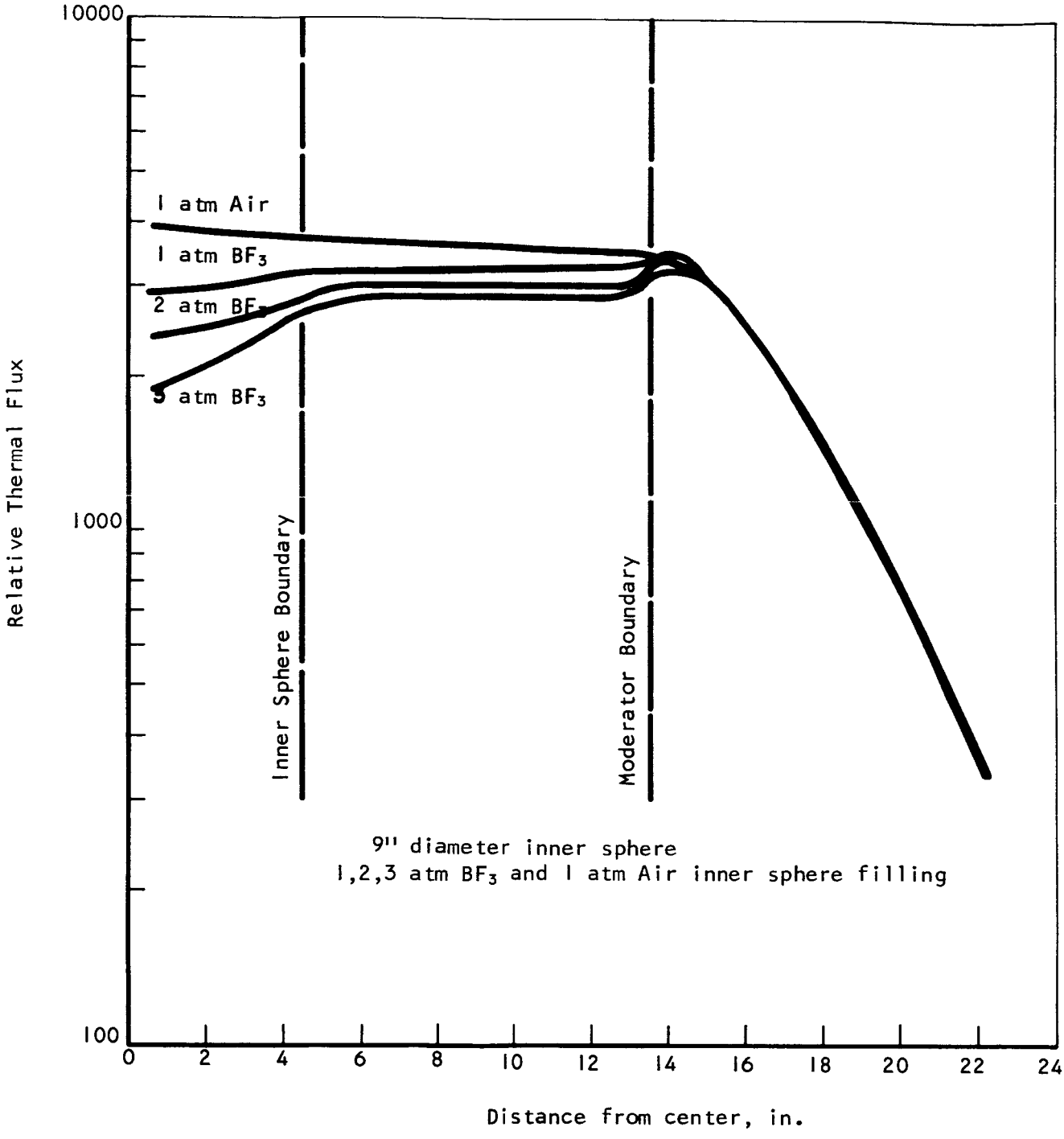

Figure 24 - Comparison of thermal flux for the 9 inch inner sphere system with various fillings.

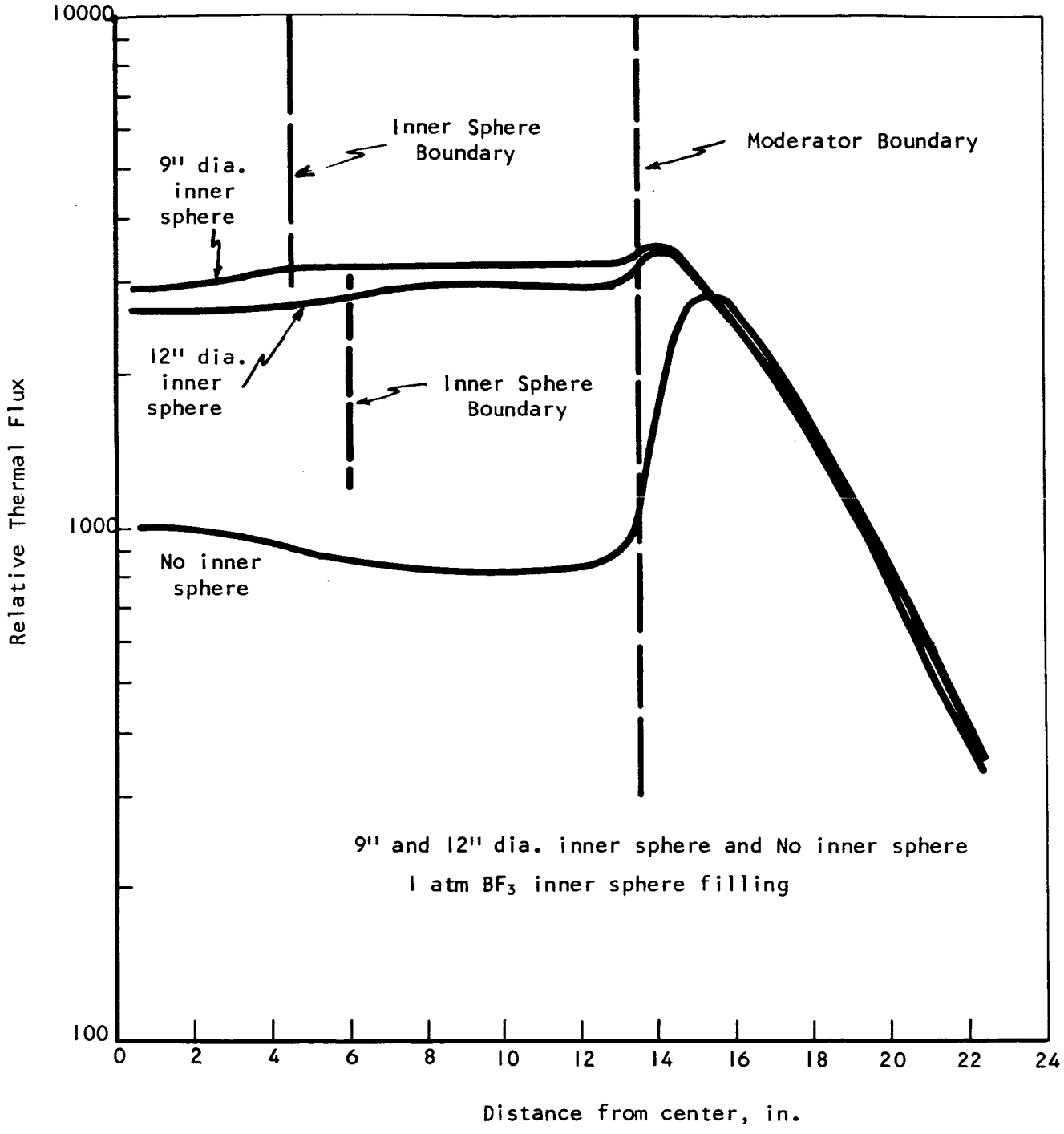

Figure 25 - Comparison of thermal flux for the three sphere systems with 1 atmosphere of BF_3 filling.

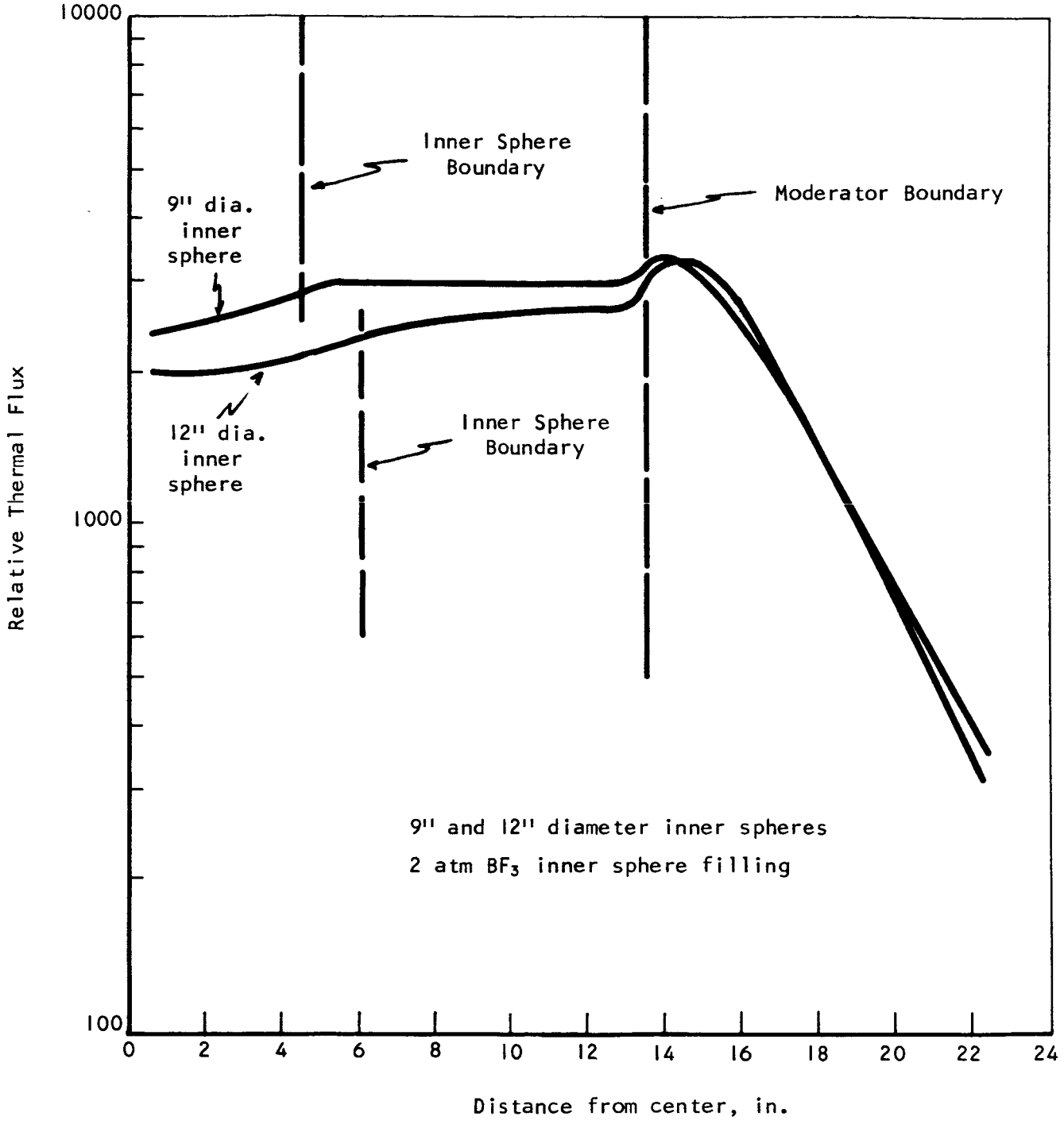

Figure 26 - Comparison of thermal flux for the 9 inch and 12 inch inner sphere systems with 2 atmospheres BF_3 filling.

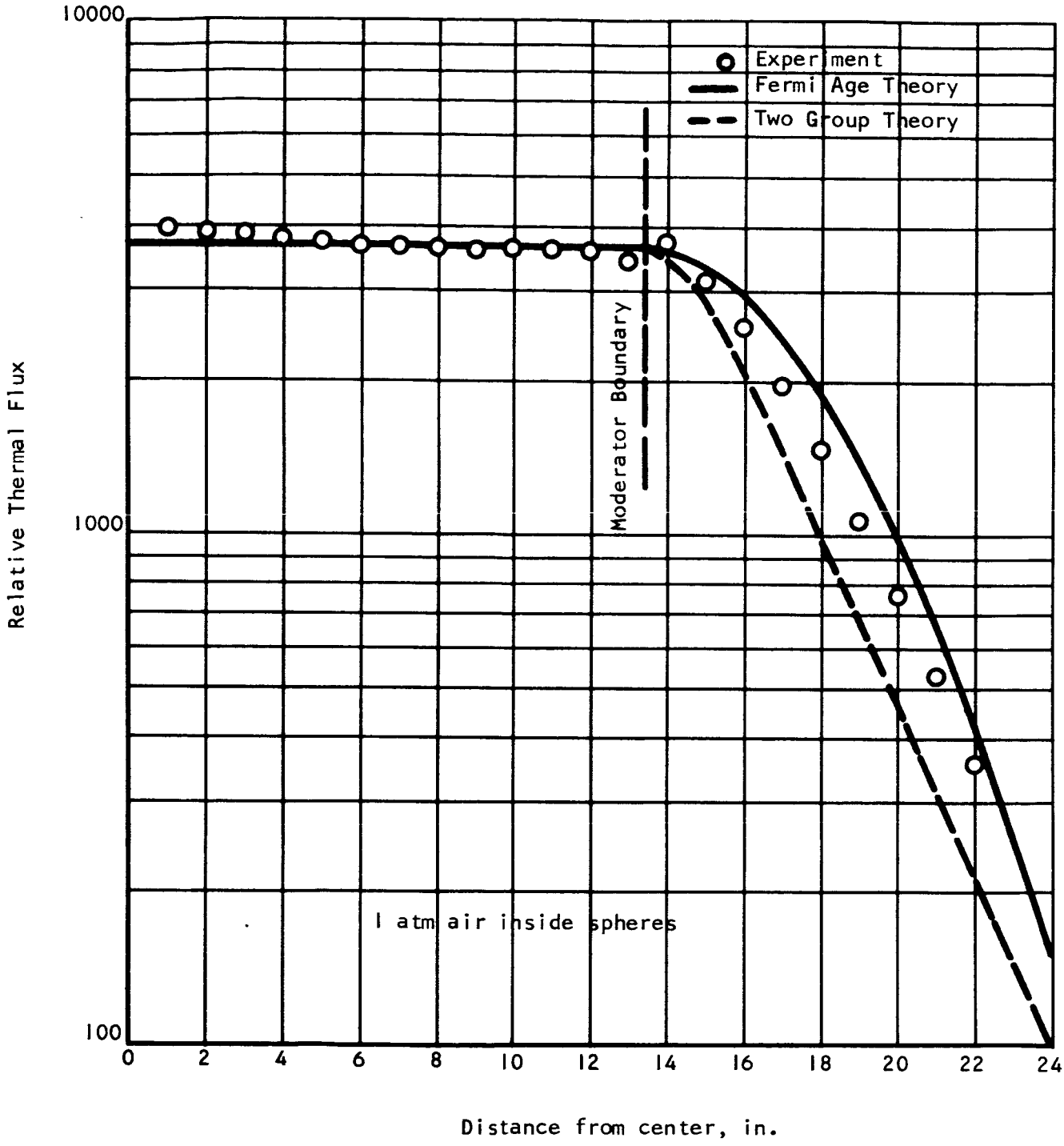

Figure 27 - Comparison of experimental and analytical flux distributions for the air filled cavity.

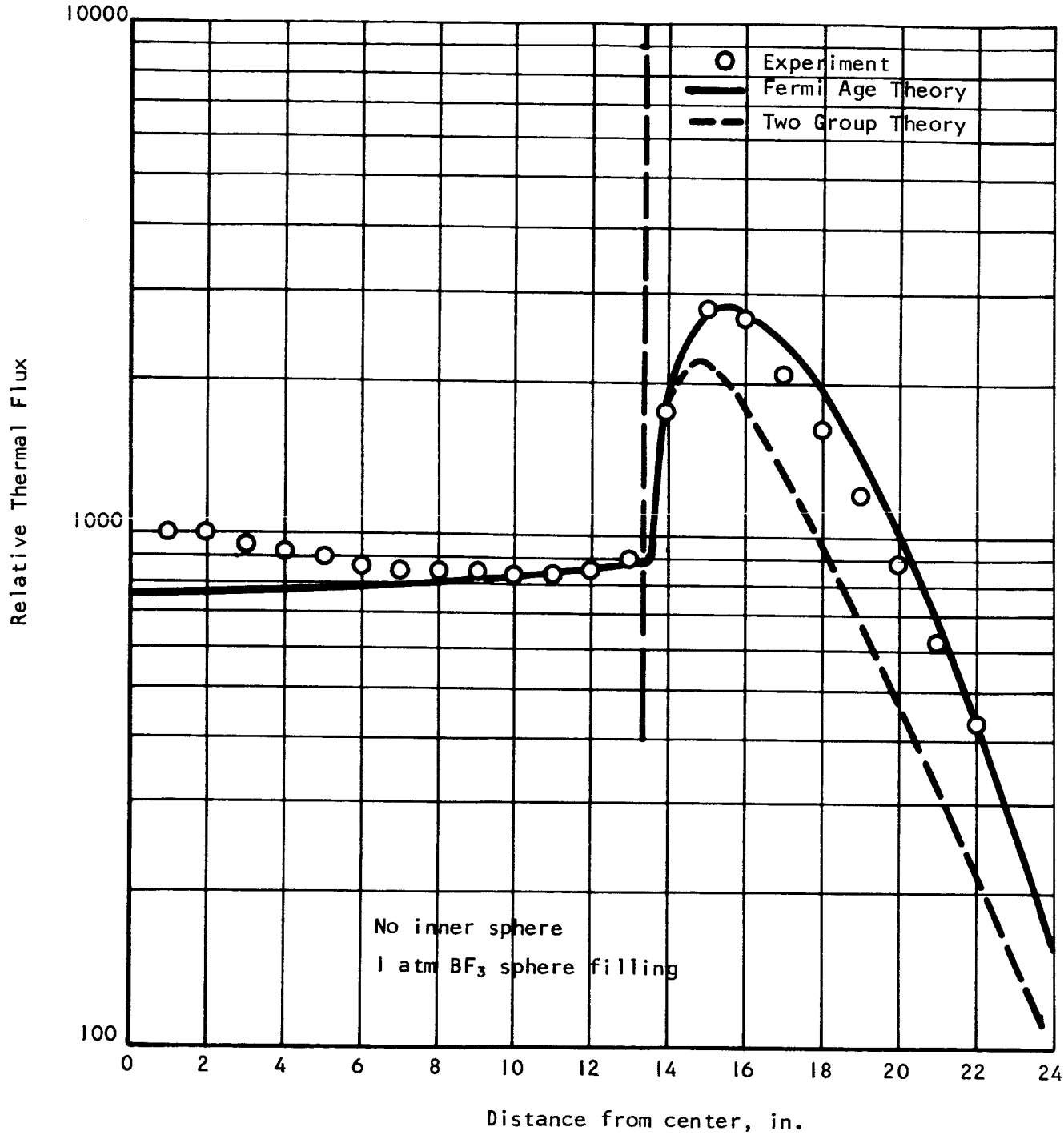

Figure 28 - Comparison of experimental and analytical flux distribution for the single sphere case with 1 atmosphere BF_3 filling.

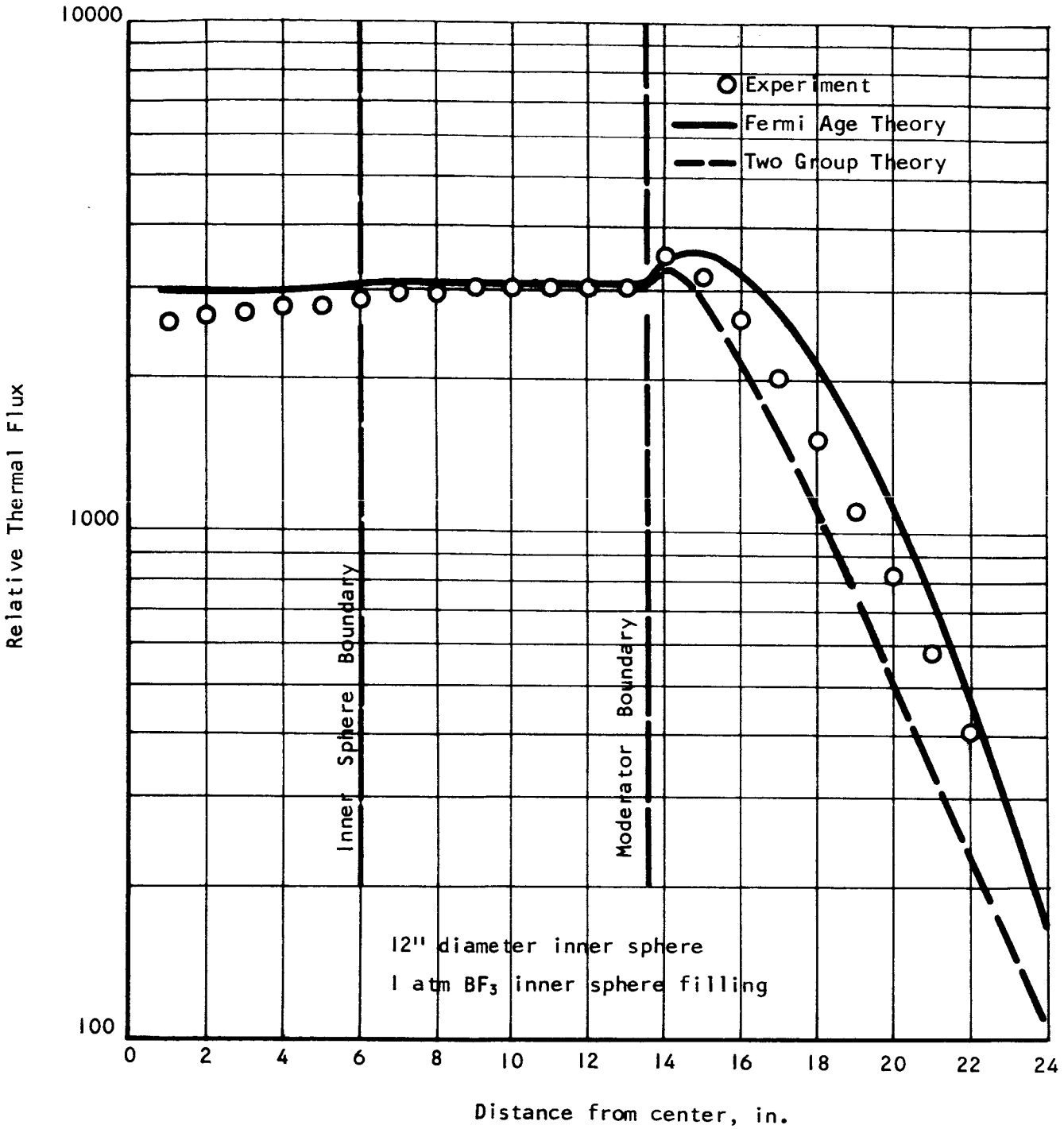

Figure 29 - Comparison of experimental and analytical flux distributions for the 12 inch inner sphere system with 1 atmosphere BF_3 filling.

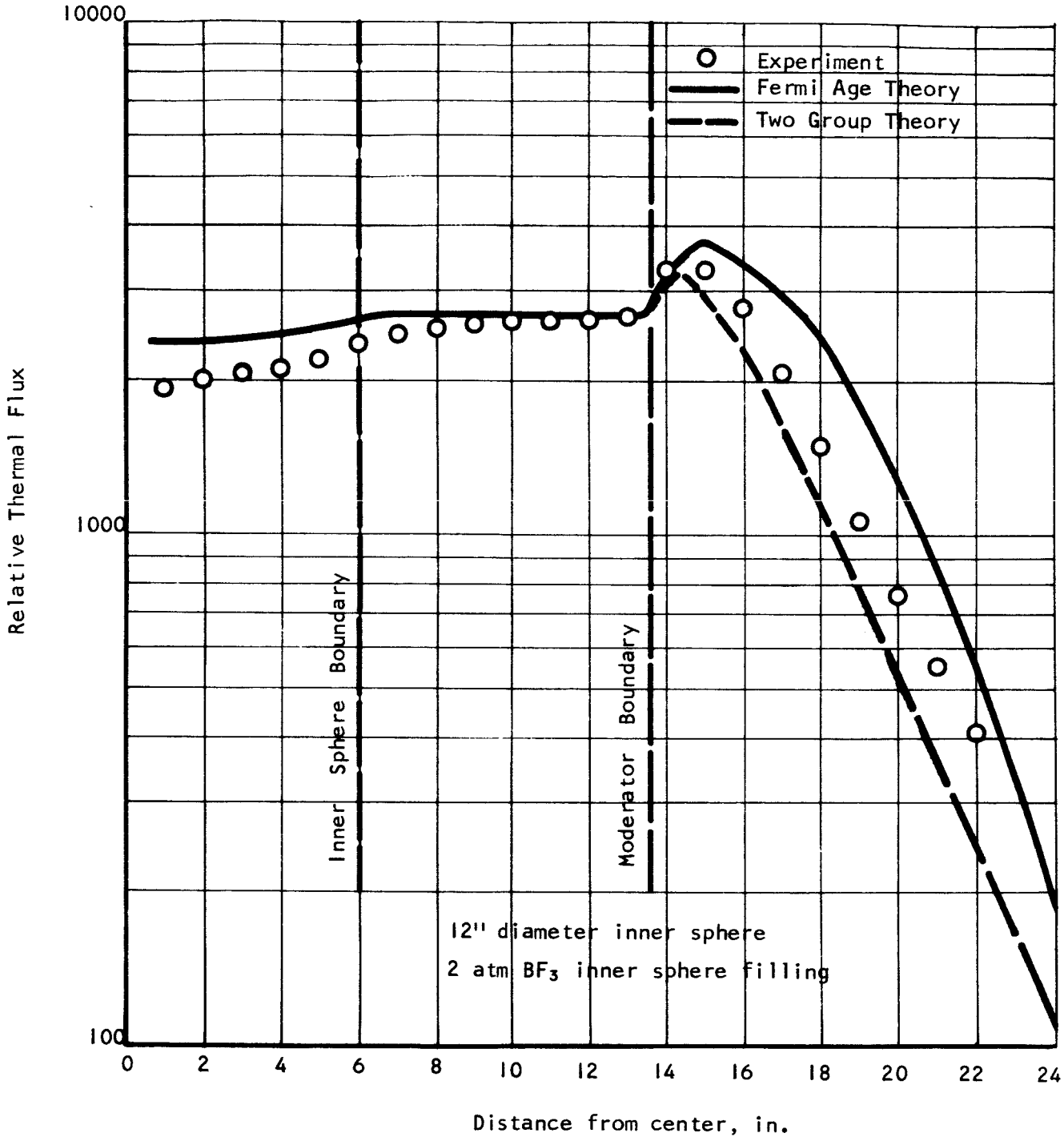

Figure 30 - Comparison of experimental and analytical flux distributions for the 12 inch inner sphere system with 2 atmospheres BF_3 filling.

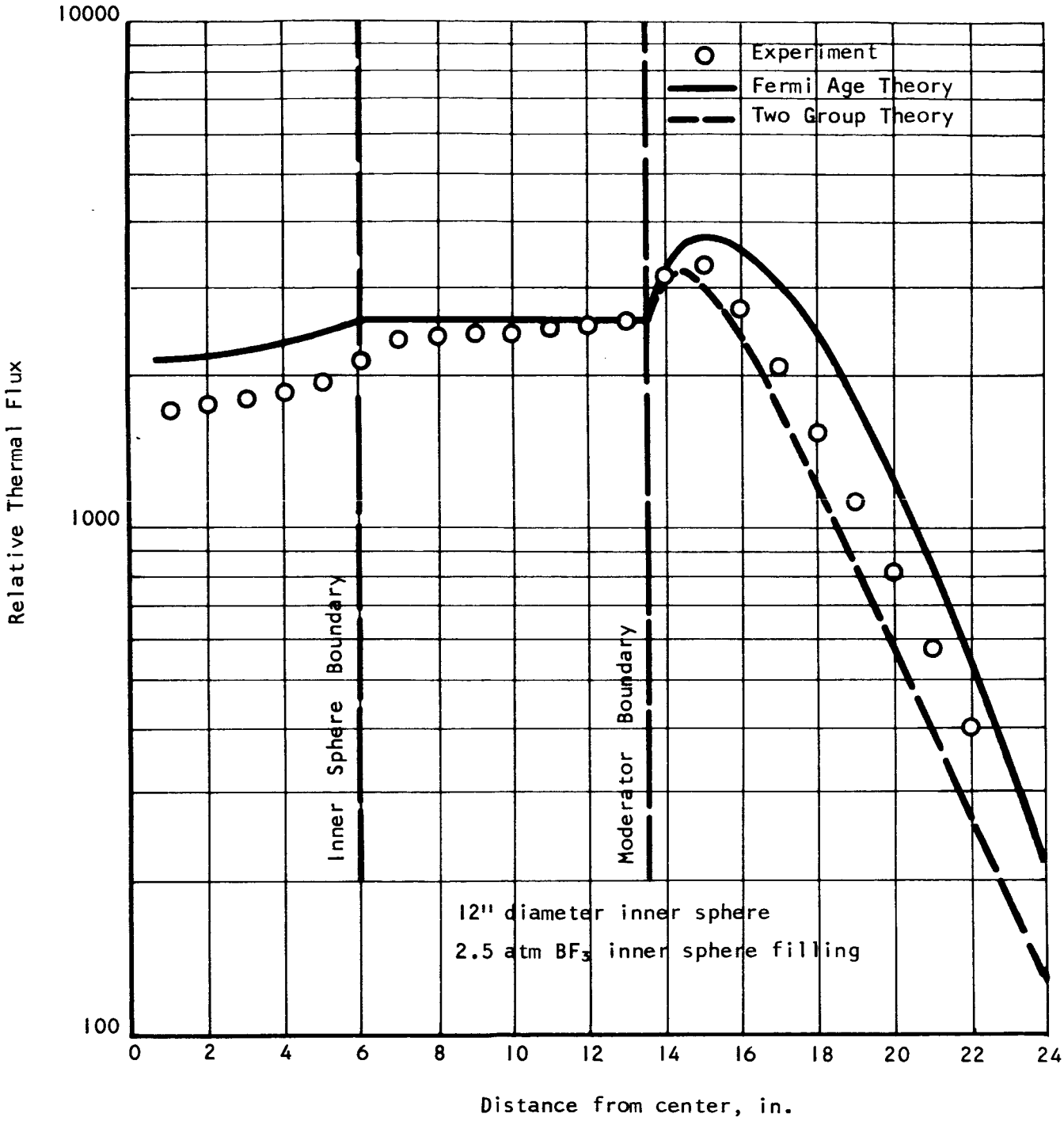

Figure 31 - Comparison of experimental and analytical flux distributions for the 12 inch inner sphere system with 2.5 atmospheres BF_3 filling.

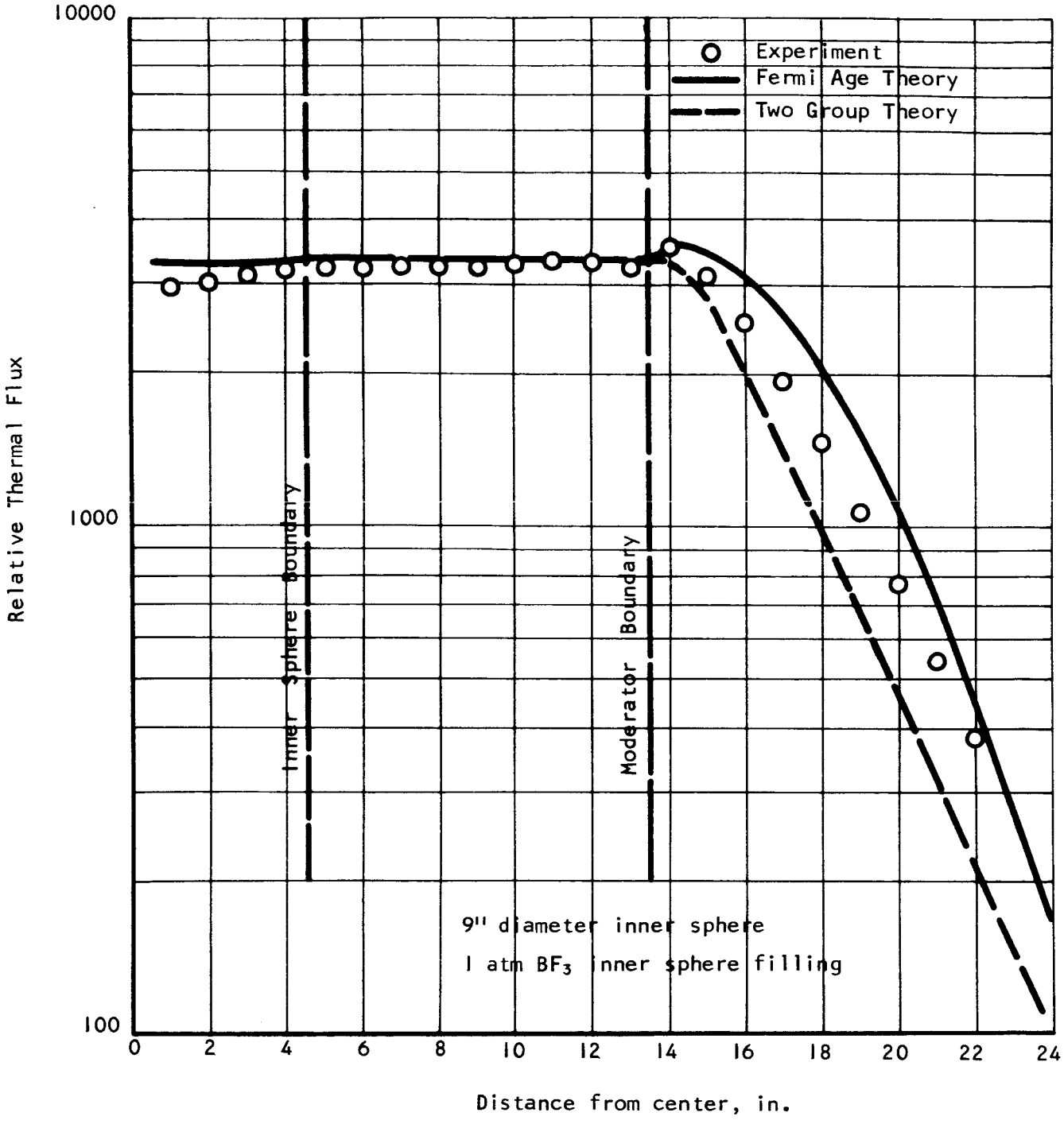

Figure 32 - Comparison of experimental and analytical flux distributions for the 9 inch inner sphere system with 1 atmosphere BF_3 filling.

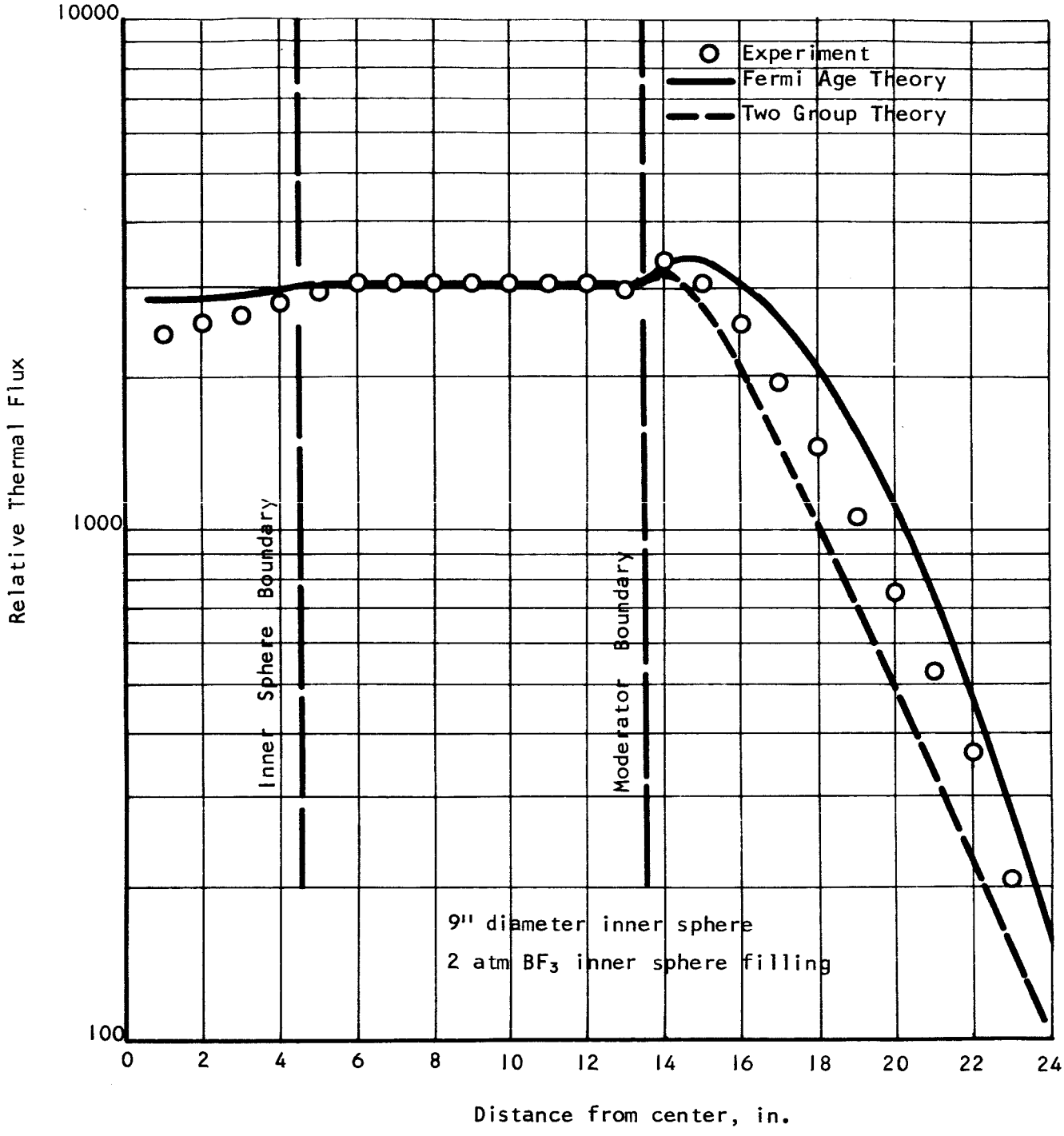

Figure 33 - Comparison of experimental and analytical flux distributions for the 9 inch inner sphere system with 2 atmospheres BF_3 filling.

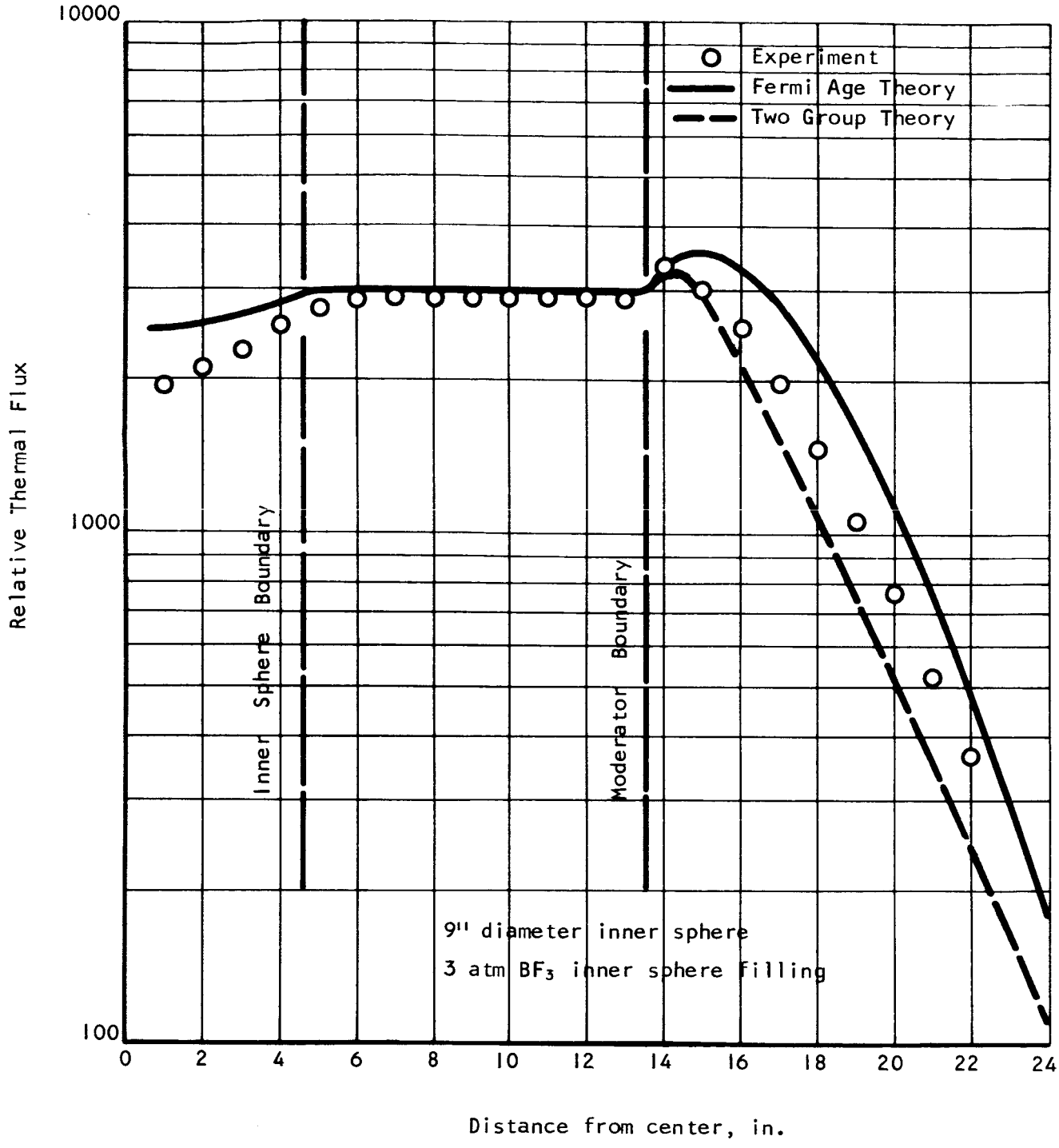

Figure 34 - Comparison of experimental and analytical flux distributions for the 9 inch inner sphere system with 3 atmospheres BF_3 filling.

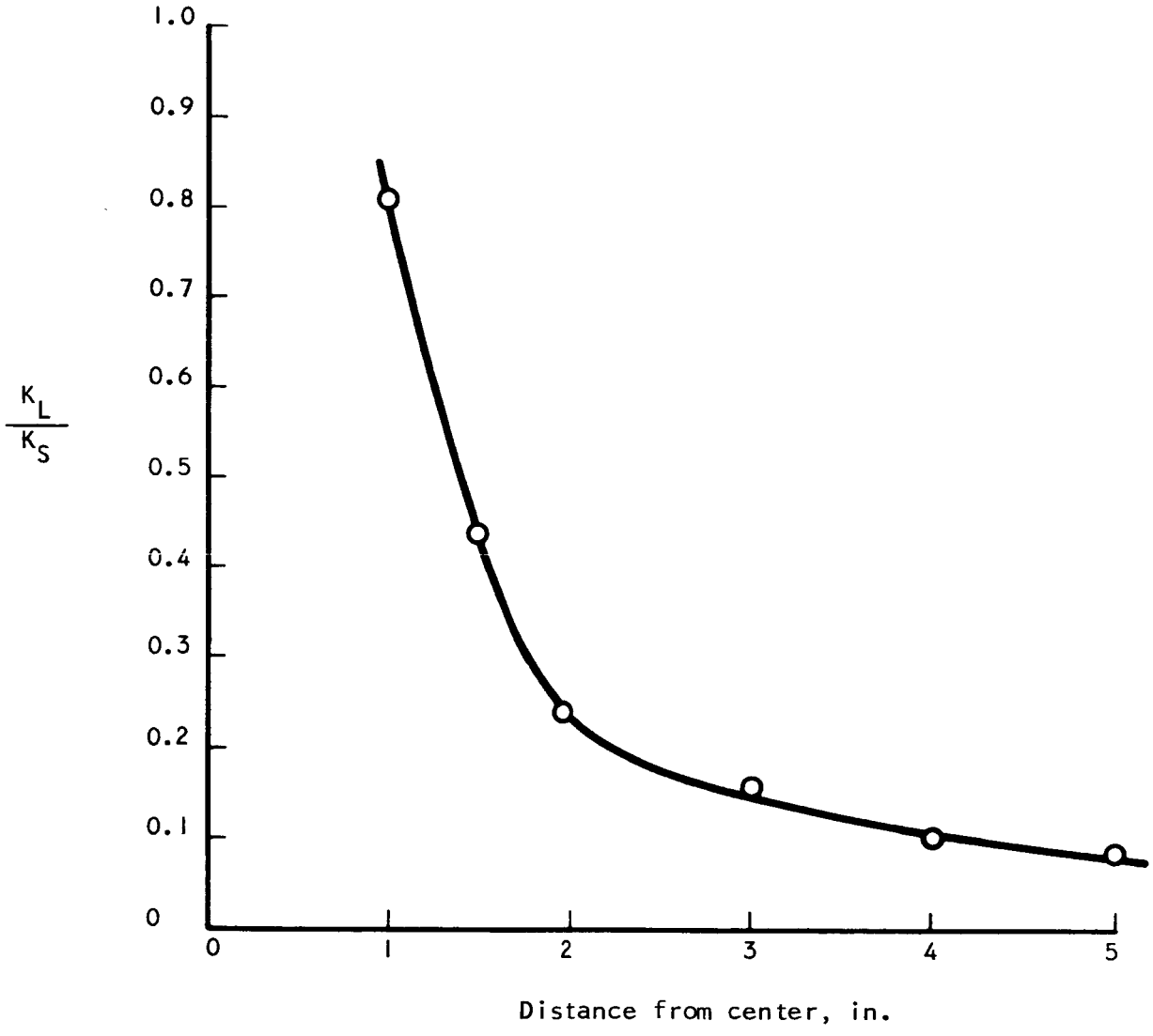

Figure 35 - Ratio of 4.50 hour to 54.3 minute activity as a function of distance from the source.

NASA Lewis Research Center (23)
21000 Brookpark Road
Cleveland, Ohio 44135
Attention: Eldon W. Sams (NRD)

NASA Lewis Research Center (1)
21000 Brookpark Road
Cleveland, Ohio 44135
Attention: Wayne E. Park (Procurement)

NASA Lewis Research Center (1)
21000 Brookpark Road
Cleveland, Ohio 44135
Attention: Normal Musial

NASA Scientific and Technical Information Facility (6)
Box 5700
Bethesda, Md.
Attention: NASA Representative

NASA Lewis Research Center (2)
21000 Brookpark Road
Cleveland, Ohio 44135
Attention: Library

NASA Lewis Research Center (1)
21000 Brookpark Road
Cleveland, Ohio 44135
Attention: Report Control Office

U.S. Atomic Energy Commission (3)
Technical Reports Library
Washington, D. C.

U.S. Atomic Energy Commission (3)
Technical Information Service Extension
P. O. Box 62
Oak Ridge, Tennessee